Palaeogeography, Palaeoclimatology, Palaeoecology 539 (2020) 109425

Contents lists available at ScienceDirect

Palaeogeography, Palaeoclimatology, Palaeoecology

journal homepage: www.elsevier.com/locate/palaeo

Ecological dynamic equilibrium in an early Miocene (21.73 Ma) forest, Ethiopia

Ellen D. Currano[a,*], Bonnie F. Jacobs[b], Rosemary T. Bush[c], Alice Novello[d,e], Mulugeta Feseha[f], Friðgeir Grímsson[g], Francesca A. McInerney[h], Lauren A. Michel[i], Aaron D. Pan[j], Samuel R. Phelps[m], Pratigya Polissar[k,l], Caroline A.E. Strömberg[e], Neil J. Tabor[b]

[a] Departments of Botany and Geology & Geophysics, University of Wyoming, 1000 E. University Avenue, Laramie, WY, 82072, USA
[b] Roy M. Huffington Department of Earth Sciences, Southern Methodist University, 3225 Daniel Avenue, Dallas, TX, 75275-0395, USA
[c] Department of Earth and Planetary Sciences, Northwestern University, 2145 Sheridan Avenue, Evanston, IL, 60208, USA
[d] Aix-Marseille University, CNRS, IRD INRA, Coll France, CEREGE, Aix en Provence, France
[e] Department of Biology, Burke Museum of Natural History & Culture, University of Washington, Seattle, WA, 98195, USA
[f] Paleoanthropology and Paleoenvironment Program, College of Natural Sciences, Addis Ababa University, Addis Ababa, Ethiopia
[g] Department of Botany and Biodiversity Research, University of Vienna, Vienna, Austria
[h] Department of Earth Sciences and Sprigg Geobiology Centre, University of Adelaide, Adelaide, SA, 5005, Australia
[i] Department of Earth Sciences, Tennessee Tech University, 1 William L Jones Drive, Cookeville, TN, 38505, USA
[j] Don Harrington Discovery Center, 1200 Streit Drive, Amarillo TX, 79106, USA
[k] Lamont-Doherty Earth Observatory, 61 Route 9W, Palisades, NY, 10964, USA
[l] Ocean Sciences Department, University of California Santa Cruz, 1156 High Street, Santa Cruz, CA, 95064, USA
[m] Department of Earth and Environmental Sciences, Columbia University, New York, NY, 10027, USA

ARTICLE INFO

Keywords:
Mush Valley
Paleobotany
Paleoenvironmental proxies
Phytoliths
n-Alkanes
Africa

ABSTRACT

Miocene paleoecology of East Africa has implications for human origins and understanding the vicariant legacy forests found today on either side of the East African Rift. Fossil leaves preserved in 21.73 million year old lacustrine sediments from the Mush Valley, Ethiopia, provide a unique opportunity to investigate forest composition and dominance-diversity patterns at an ecological scale. We classified and analyzed 2427 leaves in total from two to three quarries within each of six stratigraphic levels, spanning 7 m of section; we estimate each quarry census represents one to three centuries, and 50–60 kyrs separate the oldest and youngest levels. Pollen, phytolith, and compound-specific organic geochemical data were also collected in a detailed stratigraphic context to provide independent, integrated lines of evidence for landscape evolution and lacustrine paleoecology of the system that preserves the macrofossils. Forty-nine leaf morphotypes were documented, and Legume 1 dominated all samples. Nonmetric multidimensional scaling, Jaccard similarity analyses, and diversity and evenness indices demonstrate a degree of change comparable to community ecology dynamics, likely illustrating a dynamic stable state in forest vegetation surrounding the lake. Taxonomic assessments of leaves, phytoliths, and pollen are consistent with a closed canopy forest with limited palm diversity. A high abundance of des-A ring triterpenoid molecules (diagenetic products formed by microbial degradation under anoxic conditions) and very negative $\delta^{13}C$ values ($< -45‰$) of several hopanoid compounds point to anoxic conditions at the lake bottom, consistent with exquisite fossil preservation. The proportion of mid-chain *n*-alkanes is low, signifying relatively few submerged plants, but increases up-section, which signals shallowing of the paleolake. The Mush Valley locality is unique in Africa with regard to its very early Miocene age and the abundance and quality of organic remains. This densely forested landscape in an upland volcanic region of the Ethiopian Plateau showed resilience amid volcanic eruptions and had botanical affinities with species found today in West, Central, and eastern Africa.

* Corresponding author.
E-mail addresses: ecurrano@uwyo.edu (E.D. Currano), bjacobs@smu.edu (B.F. Jacobs), rosemary.bush@northwestern.edu (R.T. Bush), novelloalice@gmail.com (A. Novello), mulugetafyg@gmail.com (M. Feseha), fridgeir.grimsson@univie.ac.at (F. Grímsson), cesca.mcinerney@adelaide.edu.au (F.A. McInerney), lmichel@tntech.edu (L.A. Michel), apan@dhdc.org (A.D. Pan), sphelps@ldeo.columbia.edu (S.R. Phelps), ppolissa@ucsc.edu (P. Polissar), caestrom@uw.edu (C.A.E. Strömberg), ntabor@smu.edu (N.J. Tabor).

https://doi.org/10.1016/j.palaeo.2019.109425
Received 11 July 2019; Received in revised form 23 October 2019; Accepted 24 October 2019
Available online 02 November 2019

1. Introduction

Early Miocene paleoenvironmental reconstructions for tropical Africa hold significance at several scales. At the global scale, this time interval marks the development of a land connection between Africa and Eurasia (Gheerbrant and Rage, 2006; Koshnaw et al., 2018) and the biogeographical events related to that, including major faunal exchange (e.g., Ducrocq and Boisserie, 2010; Rasmussen and Gutierrez, 2009). Additionally, global climate change took place across the Paleogene-Neogene boundary, possibly related to the land connection, and to the more permanent development of Antarctic glaciers (e.g., Zachos et al., 2008). At a continental to regional scale, Neogene environments of tropical Africa are relevant to human family origins, which may be rooted in the early Miocene (Maclatchy, 2004). Furthermore, the early Miocene is a time of active tectonism and incipient rift development in East Africa, which ultimately had significant impacts on biogeography and evolution. Early Miocene topographic complexity is poorly known, but the main East African rift grabens had not yet developed (Chorowicz, 2005; Macgregor, 2015).

Early Miocene paleobotanical remains from Ethiopia provide an opportunity to document pre-rift vegetation, hypothesized to have been part of pan-tropical forests before rift rain shadows caused the development of East-West vicariants among both plants and animals (Faden, 1974; Tolley et al., 2011). This idea is borne out for specific clades, but for others is shown to be too simplistic because phylogenies of disjuncts indicate splits both earlier and later (Couvreur et al., 2008; Plana, 2004; Sosef, 1996). Closer paleoecological sampling of fossil plants and isotopic data is required to resolve early Miocene temporal and spatial variation among communities and attendant paleoclimate. To date, the earliest Neogene East African paleofloras, estimated to be 20–18 Ma (Peppe et al., 2011), were reported from sites on Rusinga Island in Lake Victoria, western Kenya. While Rusinga has provided vital information, paleoenvironmental information has long been almost entirely lacking for East Africa earlier in the Miocene.

In this paper, we begin to fill this gap by reporting on paleoecological analyses incorporating plant macrofossils, phytoliths, pollen, and compound-specific carbon isotope ratios, from the Mush Valley, Ethiopia, dated at 21.73 Ma (Tesfamichael et al., 2017). The exceptional preservation and abundance of Mush Valley plant macrofossils, which occur in carbonaceous lacustrine shales, allow us to characterize plant community ecology on a decadal to millennial time scale, measuring richness, dominance-diversity patterns, and heterogeneity, spatially, by sampling from a single stratum, and temporally, by sampling up-section. These data, complemented by taxonomic identifications, phytolith assemblages, and geochemical analyses, set a standard for analysis of a rich, mulit-proxy view of paleoenvironment and can be compared in some detail with other well preserved Cenozoic African paleofloras to assess large-scale abiotic and biotic change.

2. Materials and methods

2.1. Geologic setting

The Mush Valley site (9°47′ N, 39°39’ E) is located on the Ethiopian Plateau ~160 km northeast of Addis Ababa, approaching the western shoulder of the Main Ethiopian Rift (Fig. 1). The site is 2700 m above sea level surrounded by agricultural land, once vegetated by “dry evergreen Afromontane forest and grassland complex” (Friis et al., 2010; classified by White [1983] as undifferentiated montane vegetation). It is geographically, and very likely geologically, related to the early Miocene Guguftu shield volcano described by Kieffer et al. (2004), who provided a range of ages from a variety of outcrop samples of alkaline basalts, a majority of which are ~23-22 Ma. At the Mush Valley site, abundant plant, insect, fish, and frog compression fossils, and, less commonly, the bones of mammals and crocodiles are preserved in a stratigraphic sequence exposed by the modern Mush River. Fossils

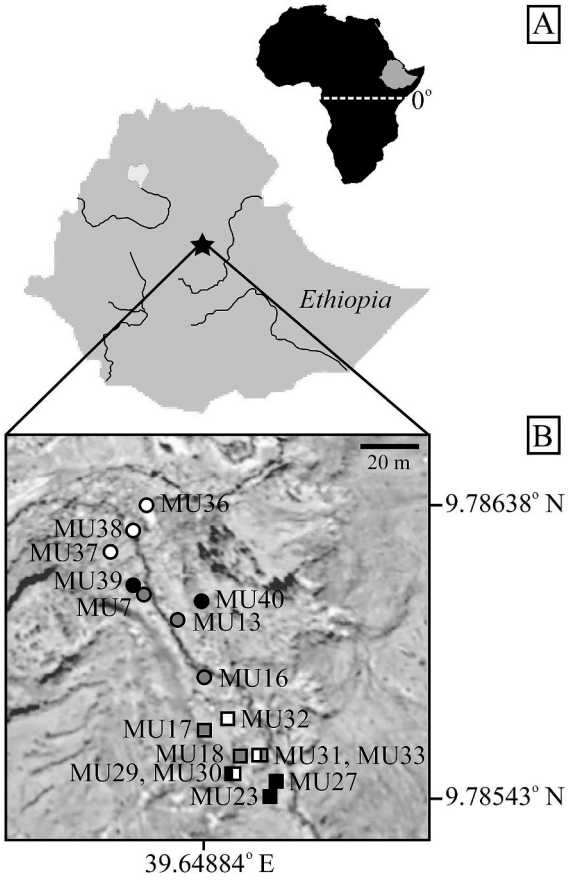

Fig. 1. Geographic location of the Mush leaf quarries in Ethiopia (A). The fossiliferous strata are exposed along the modern-day Mush stream, imaged using Google Earth (B). Level A quarries are white circles, Level B gray circles, Level C black circles, Level D white squares, Level E gray squares, and Level F black squares. The location of quarries MU31 and MU33 cannot be distinguished at this resolution, nor can MU29 and MU30.

occur in carbonaceous shales interbedded with volcanic ash layers. With the exception of a 10 cm thick ash that occurs midway through the fossiliferous section (Fig. 2; Level C), ash beds are generally 1–3 cm thick. Zircons from ashes immediately below the fossiliferous units and 5 m below that, respectively, yielded two $^{238}Ur/^{206}Pb$ dates: 21.733 ± 0.060 (0.06) [0.07] Ma and 21.736 ± 0.015 (0.03) [0.03] Ma (Fig. 2; Tesfamichael et al., 2017).

The biotic interpretation of the Mush Valley assemblages to date envisions a closed-canopy, mixed-moist semi-evergreen forest (Bush et al., 2017; Pan et al., 2012; Pan et al., 2014). Mean annual precipitation at Mush, reconstructed using leaf area analysis as 1523–1647 mm/yr, is comparable to that in the modern mixed-moist semi-evergreen rainforests that cover most of the Guineo-Congolian region; it is too high for woodland or bushland ecosystems (Bush et al., 2017; White, 1983). Moreover, fossil leaf stable carbon isotope ($\delta^{13}C$) values from Mush Valley samples average −29.1‰, which best matches the average for modern tropical rain forests after correcting for $\delta^{13}C$ of atmospheric CO_2 (Bush et al., 2017; Diefendorf et al., 2010), and the genera *Newtonia* and *Tacca*, found today in moist tropical or secondary forests, were identified at Mush (Pan et al., 2012).

2.2. Fieldwork and plant macrofossil analyses

A stratigraphic section spanning the lacustrine shales was measured at the centimeter scale. Unbiased, quantitative plant censuses, or counts of every identifiable leaf(let) with at least half of the blade preserved, were conducted at six stratigraphic levels within this section (Fig. 2):

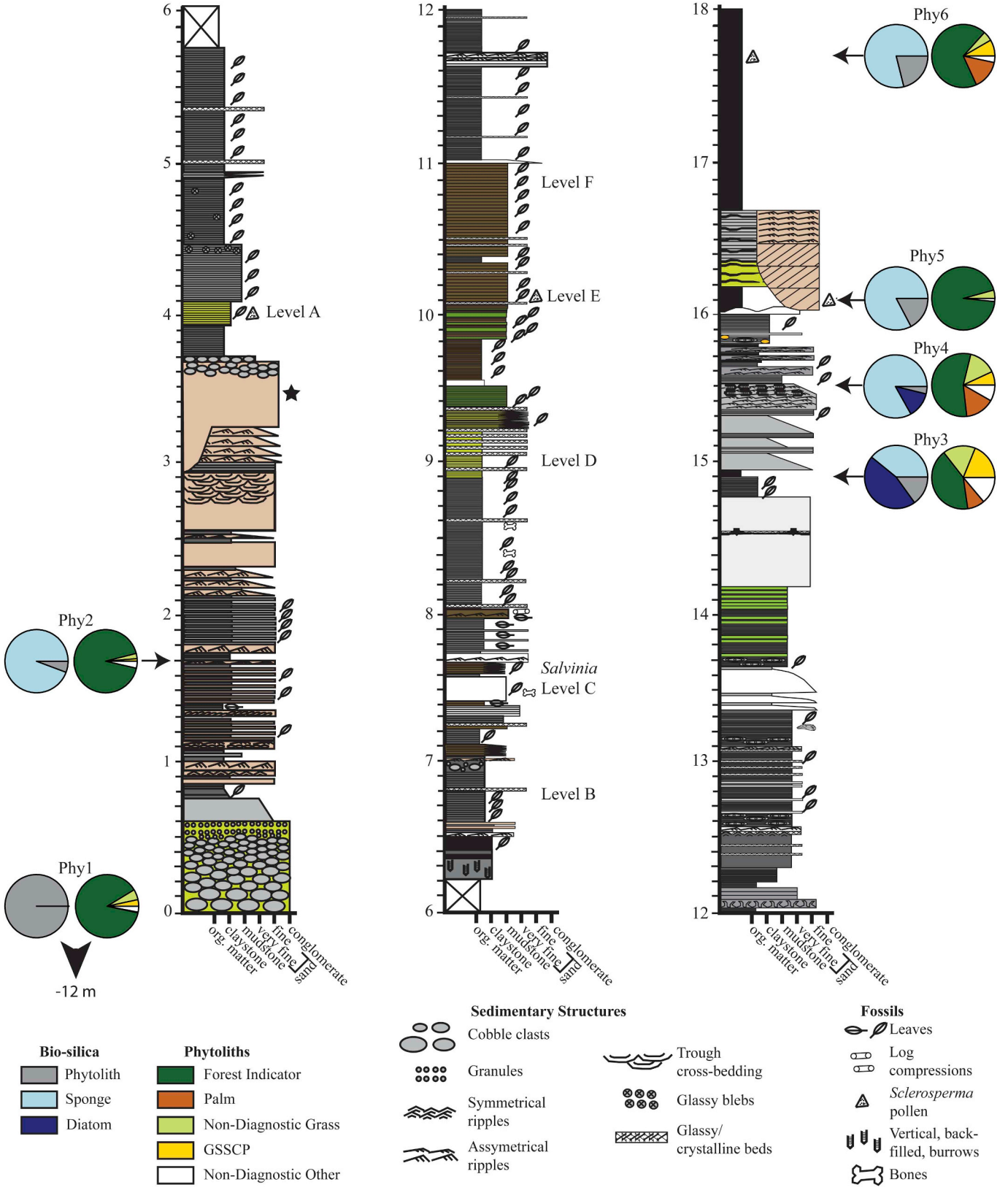

Fig. 2. Detailed stratigraphic column through the Mush fossil beds, modified from Bush et al. (2017). Stratigraphic levels at which leaf macrofossil censuses were conducted are labeled, as in "Level A." Stratigraphic levels at which phytolith analyses were conducted are labeled Phy1-Phy6, and pie charts summarize the biosilicate (left) and phytolith (right) assemblage composition. GSSCP stands for Grass Silica Short Cell Phytoliths. The star indicates the stratigraphic height of the 21.73 ± 0.03 Ma $^{238}U/^{206}Pb$ date (Tesfamichael et al., 2017). Fossil animal material was collected at the three stratigraphic levels indicated by the bones; only the upper two levels preserve frog melanosomes. Laminated carbonaceous shales are interpreted as lacustrine and are interbedded with thin, asymmetrically rippled sandstones in the lowest 2 m of section and cm-scale ash beds above. The onset of lacustrine conditions is interrupted by deposition of water-reworked ash from about 2.55 to 3.7 m. Siltstones and fine sandstones with asymmetrical ripples, burrows, and plant fossils occurring between 12 and 16.7 m are interpreted as shallow lacustrine or deltaic deposits.

two carbonaceous shale horizons below the 10 cm thick ash bed (Levels A and B), within the ash bed itself (Level C), and three shale horizons above the ash bed (Levels D-F). These levels, which span ~7 m of section, were chosen because they contained abundant and high quality leaf remains and could be traced laterally in order to collect replicate samples. The fossiliferous shales are exposed along a cut of the Mush stream, and were excavated adjacent to it. This steep, small valley is spring-fed and perpetually wet, a circumstance that helps maintain excellent preservation by retarding natural shrink-swell physical weathering of the clay-rich matrix. Because fossiliferous blocks quickly crack when exposed to dry air and intense sunlight, leaves were not censused in the field. Rather, a 5-cm thick layer with a surface area of approximately 1.5 × 1.5 m was excavated from each level. Three laterally equivalent quarries were excavated per stratigraphic level for five of six levels (A,B,D,E,F), with quarry locations chosen based upon accessibility of the 5-cm layer. Only two quarries were collected at Level C due to lower fossil density and time constraints. All quarries are within 120 m of each other, and the maximum lateral distance between quarries within a stratigraphic level is 35 m (Fig. 1; Table S1).

Fossiliferous blocks were wrapped in paper immediately after excavation and remained wrapped for about six months to dry slowly. Blocks were unwrapped and studied at the National Museum of Ethiopia, Addis Ababa. All fossil material exposed on each block exterior was analyzed first, and then blocks were split along bedding planes using chisels, knives, and hammers in order to expose additional fossils. Leaf fossils were sorted into plant morphotypes using leaf architectural (Ellis et al., 2009) and cuticular characters (Dilcher, 1974). Cuticular characters were studied on small chips collected from fossils that could not be identified using leaf architectural characters alone. Samples were examined using epifluorescence and digital imaging (see Supplemental Information). All fossils are curated at the National Museum of Ethiopia, Addis Ababa, and cuticle specimens are curated at Southern Methodist University.

A total of 2427 fossil leaves were classified into morphotypes and included in ecological analyses. Other plant organs such as seeds and fruit were omitted from quantitative analyses, as they could not be assigned to any leaf taxon with certainty. Although *Tacca umerii* is the only leaf morphotype that has been assigned a scientific name, we are confident that all our leaf morphotypes are distinct from one another based upon unique combinations of leaf architectural and cuticular characters. Morphotypes were assigned informal names (e.g., "Short Drip Tip" or "Long&Loopy") to help our team remember key features of each morphotype and to aid in communication, and these names are attached to the specimens at the National Museum of Ethiopia. Key features of each morphotype are included in the Supplemental Materials (Table S6).

Quantitative analyses were conducted using RStudio Version 0.99.789 (©2009–2016 RStudio, Inc.). We analyzed plant composition, species richness, evenness, and heterogeneity at increasingly inclusive scales: individual quarry, stratigraphic level, and the entire Mush dataset (Fig. 3). Nonmetric multidimensional scaling (NMDS) ordinations were conducted to examine floristic similarities among sites using arcsine square root transformed morphotype abundance data and R's "metaMDS" function with Bray-Curtis distance specified (McCune and Grace, 2002). Species richness at specific sample sizes (rarefied richness) was determined using analytical rarefaction (R's "rarefy" function; Oksanen et al., 2016), and errors were estimated using Heck et al.'s (1975) standard error. Pielou's J was computed to compare evenness among different floras, and Jaccard's similarity coefficient was used to analyze species heterogeneity among sites.

We partitioned diversity at Mush into quarry-level diversity (α_q), among-quarry diversity within a stratigraphic level (β_w), and among stratigraphic level diversity (β_b; Fig. 3). Floral diversity was quantified using Hill numbers, or "effective number of species," which is defined as the number of equally abundant species needed to produce the given value of the diversity index (Jost, 2007). Hill numbers have only rarely been used in paleoecological studies, but they are considered the standard for ecologists working on extant systems (Chao et al., 2014; Ellison, 2010). Hill numbers are the "numbers equivalents" of traditional diversity estimates (e.g., Shannon, Simpson) and represent true diversities rather than entropies (Jost, 2007). Thus, they are more in tune with biological intuition about the magnitude of diversity changes than either Shannon or Simpson indices (see examples of Jost, 2007). The general formula for calculating Hill numbers is:

$$ {}^{q}D = \left(\sum_{i=1}^{S} p_i^q \right)^{1/(1-q)} \quad (1) $$

where S is the number of species at a site, p is the proportional abundance of a species, and q is the order of the diversity measure and indicates the sensitivity to rare versus common species ($q = 0$ for species richness, $q = 1$ for Shannon, and $q = 2$ for Simpson). We calculated ${}^{0}D$ (which is equal to S, or species richness) and ${}^{2}D$ (the effective number of common species in a sample).

We partitioned diversity both additively, following Lande's (1996) protocol, and multiplicatively, following Jost (2007). Additive diversity partitioning gives beta diversity (β^{+}) equal to the effective number of species within a region that are not captured by a single sample and thus maintains the magnitude of diversity differences. Multiplicative diversity partitioning provides a beta diversity ($\beta^{\times}$) that represents the effective number of unique communities within a region; $\beta^{\times}$ is strictly independent of alpha diversity (Chao et al., 2012). A thorough description of calculation methods is included in the Supplemental Materials.

2.3. Phytolith analyses

Twenty-three sediment samples were processed for phytoliths using the protocol initially developed by Strömberg (2003) and subsequently improved by Strömberg et al. (2013) (See Supplemental Information). Initial observations were made at 400× magnification and, if necessary, counting was done at 1,000× magnification. Immersion oil mounts were made to count the Grass Silica Short Cell Phytoliths

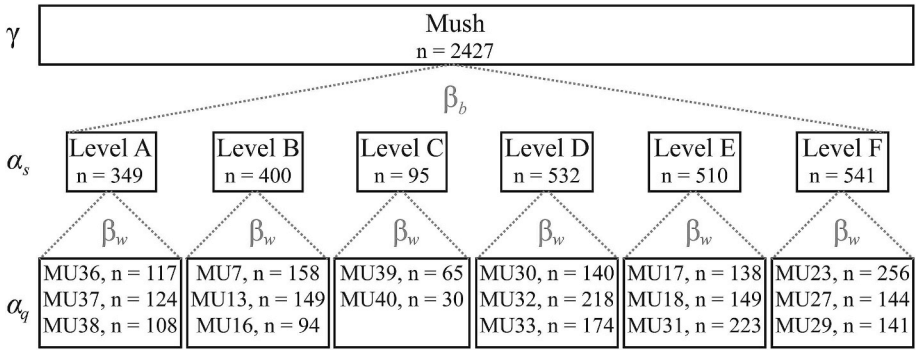

Fig. 3. Sampling scheme at Mush, illustrating how diversity is partitioned. α_q is the diversity at an individual quarry, and α_s is diversity at an individual stratigraphic level. β_w is within-stratigraphic level turnover diversity, and β_b is among stratigraphic level turnover diversity. Total species diversity at Mush is given by γ. The MU numbers indicate sublocalities, and Levels A-F are marked on the stratigraphic column in Fig. 2. The number of identifiable leaf specimens in a sample is denoted by n.

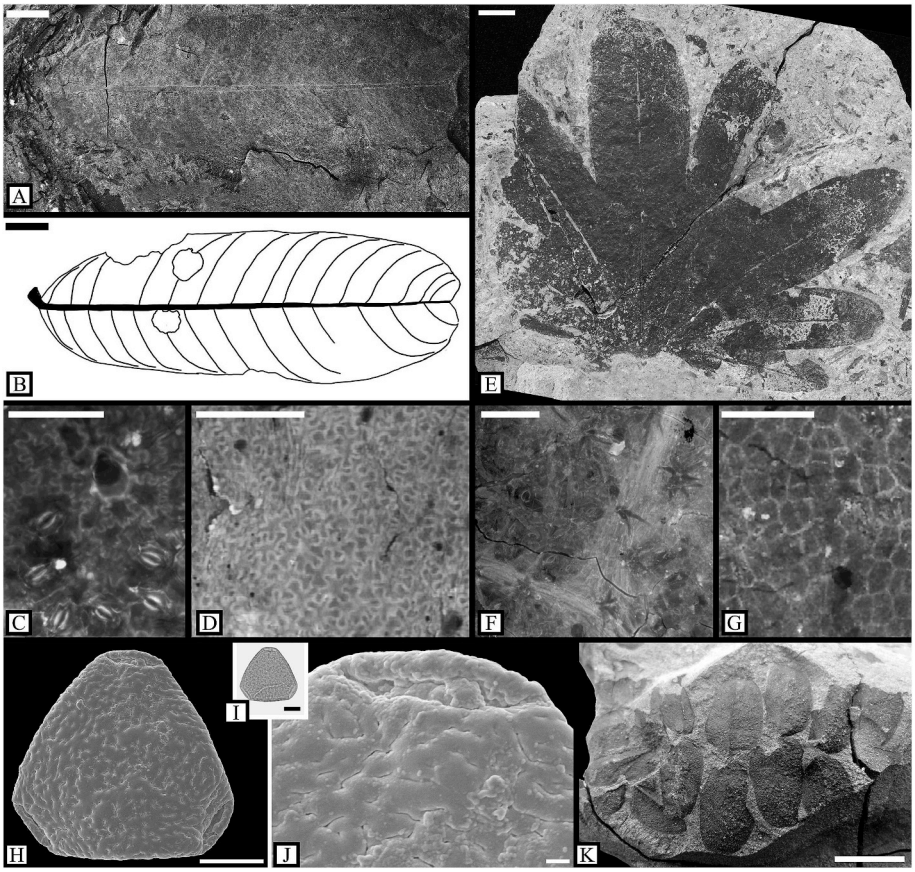

Fig. 4. Paleobotanical remains discussed in the text. "Yellow leaf" dicot morphotype, specimen MU36-21 #1 (A) and accompanying line drawing (B), adaxial cuticle (C; MU33-18 #1), and abaxial cuticle (D; MU38-27 #1). *Tacca umerii* leaf (E; MU22-29), adaxial cuticle (F; MU30-34B #1), and abaxial cuticle (G; MU37-16B). *Sclerosperma* (Arecaceae) pollen (H-J; sample Phy6). The sediments just above Level C, at approximately 7.6 m in the measured section, contain abundant *Salvinia* fossils (K; MU20-1). Scale bars are 1 cm in A, B, E, and K; 50 μm in C, D, F, and G; 10 μm in H and I; and 1 μm in J.

(GSSCP), which have distinctly three-dimensional shape features and rotation is therefore necessary for robust identification. Phytolith counts include only the bodies that were sufficiently well-preserved to be described and classified; fragments or highly etched and/or altered specimens were not included (Strömberg et al., 2018). Phytolith classification followed Strömberg (2003) for non-GSSCP phytoliths; for GSSCP, we adopted schemes used by Novello (2012) and Neumann (2017) developed specifically for African grasses, supplemented by Strömberg (2003) and Piperno and Pearsall (1998) for morphotypes related to early-diverging grasses and Bambusoideae (Table S2). In addition, the reference collections of the CEREGE and the Burke Museum of Natural History and Culture were consulted for GSSCP of particular grass taxa (e.g., *Leptaspis*).

At least 200 diagnostic phytoliths were counted for each productive sample to ensure robust environmental reconstructions (Strömberg, 2005). Diagnostic phytoliths consist of three main plant functional type categories: (1) GSSCPs, exclusive to the Poaceae (grass) family, (2) forest indicator (FI: Forest Indicator) phytoliths, which mostly includes morphotypes typical of woody and herbaceous dicotyledonous angiosperms, (3) palm (Arecaceae) phytoliths, and (4) sedge phytoliths. The GSSCP were further divided into forms tentatively associated with the subfamily or clade they are diagnostic of or presently produced abundantly by, namely: (a) Pharoideae, (b) Bambusoideae, and (c) Pooideae, which all exclusively use C_3 photosynthesis, (d) PACMAD, a clade of tropical grasses containing both C_3 (e.g., Arundinoideae) and C_4 (e.g., Panicoideae) grass members, and (e) Uncertain, for GSSCP of unknown origin. To estimate the arboreal cover quantitatively, we use the D/P ratio (e.g., Alexandre et al., 1997; Bremond et al., 2005; Bremond et al., 2008), which compares the number of dicot ("D") rugose sphere indicators (also called granulate by the previous authors) to the number of GSSCPs diagnostic to Poaceae ("P"). The format $D/(D + P) \times 100$ was preferred so that the values are scaled between 0 and 100. Using the D/P ratio allows for comparison with the comprehensive body of modern analog work in Africa (Barboni et al., 2007; Novello et al., 2017). We also calculated the FI-t ratio, which estimates arboreal cover using all identified forest indicator phytoliths, not just the rugose spheres. Calculating this index allows us to compare to studies of similarly-aged floras on other continents (e.g., Harris et al., 2017; Strömberg et al., 2013; Strömberg, 2004, 2005). Other phytolith morphotypes were classified into two main categories: (4) NDG (Non Diagnostic Grass), which includes non-GSSCP grass phytoliths, morphotypes produced in abundance by grasses but also by other monocotyledonous plants, and/or conifers (including, e.g., silicified bulliform cells, trichomes, and spiny elongates), and (5) NDO (Non Diagnostic Other), which are non-diagnostic phytoliths produced by a wide range of plants (i.e., of unclear origin). Because of the taxonomic uncertainty associated with some NDG forms and because the silicification of bulliform cells, trichomes, and elongates by herbaceous plants varies greatly with abiotic factors such as water supply and evapotranspiration rates (Madella et al., 2009; Sangster and Parry, 1969), these morphotypes were not used to estimate arboreal cover. Sedge phytoliths are often used to indicate wetland elements or proximity to water (see Strömberg, 2004; Strömberg et al., 2018); here we included them as herbaceous indicators (Table S2). Other bio-silica remains, such as diatom frustules and sponge spicules, when observed, were also counted. In this case, only spicules > 10 μm-long and complete diatom frustules were included in the count. These biosilica components are strong indicators of different lake environments or environmental humidity (Clarke, 2003).

2.4. Pollen preparation

Sedimentary rock samples from Level B (quarry MU7, 4.0 m in the section), Level E (MU18, 10.1 m), Phy5 (16.1 m), and Phy6 (17.7 m) were processed and fossil pollen grains extracted according to Grímsson et al. (2008). All samples were especially screened for palm pollen. The

Table 1
Floral diversity at evenness at Mush.

	Level A	Level B	Level C	Level D	Level E	Level F	TOTAL
# Quarries	3	3	2	3	3	3	17
# Leaves	349	400	95	532	510	541	2427
# Leaf Morphotypes	26	32	14	37	31	25	49
Mean annual precipitation[a]	1638, +214, −125	1583, +207, −121	–	1523, +199, −116	1608, +211, −123	1597, +209, −122	1647, +216, −126
Richness of strat level, 300 leaves[b]	25.0 ± 0.9	28.8 ± 1.5	–	30.9 ± 2.0	27.0 ± 1.6	20.4 ± 1.7	28.6 ± 2.4
Average richness of single quarry, 100 leaves[c]	17.3 ± 1.9	17.7 ± 0.1	–	18.9 ± 3.0	16.9 ± 1.0	12.6 ± 1.1	16.6 ± 2.7
Hill number (q = 2)	6.76	3.07	3.97	3.50	3.12	2.16	3.55
Pielou's J	0.50	0.38	0.49	0.39	0.38	0.31	0.36
Percent of leaves that are Legume 1	30.9	55.8	49.5	50.9	55.7	65.8	53.1

[a] Reported in Bush et al. (2017). Positive and negative error margins are unequal due to transformation from the log value.
[b] Errors estimated using the standard error of Heck (1975).
[c] Errors reported are one standard deviation around the mean of quarry richness at 100 leaves.

same palm genus, *Sclerosperma*, was observed in all four samples (Fig. 4IH–J). No other palm pollen was obtained. The fossil pollen grains were investigated both by light and scanning electron microscopy using the single grain method as described by Zetter (1989) and Halbritter et al. (2018).

2.5. Organic geochemistry

For quantification and isotope measurements of lipids, samples of fossil-bearing sediment were chipped from the larger fossil blocks, and their surfaces cleaned by chipping any previously exposed portions. Sediments were then ground to powder in a ball mill, and lipids were extracted from 5 g of pulverized sediment using the methods described in the Supplemental Information. *n*-Alkanes were identified and quantified using a ThermoFisher Trace GC Ultra fitted with a flame ionization detector (FID) and coupled to a quadrapole mass spectrometer (ThermoFisher DSQII). Compound specific carbon isotope ratios were measured at the Lamont-Doherty Earth Observatory on a Thermo Delta V advantage coupled to a Thermo Trace GC Ultra and Isolink through a ConFlo IV interface. Molecular standards purchased from Arndt Schimmelmann (University of Indiana) were measured throughout each analytical sequence and were used to determine the isotopic values of samples on the VPDB scale and their uncertainty following the methods of Polissar and D'Andrea (2014). Mixtures A4, A5, and B4 were used for calibration and the isotopic composition of the compounds is listed in Table S4. Average chain length (ACL) and carbon preference index (CPI) were calculated for all samples (see Supplemental Information). Following Ficken et al. (2000), a proxy for submerged and floating aquatic macrophytes versus emergent macrophytes and terrestrial plants, P_{aq}, was calculated as

$$P_{aq} = (C_{23} + C_{25})/(C_{23} + C_{25} + C_{29} + C_{31}) \quad (2)$$

3. Results

3.1. Stratigraphic context

The measured section represented in Fig. 2 overlies approximately 10 m of ignimbrite containing charcoalized wood, including a large *in situ* tree in upright growth position. This ignimbrite directly overlies a paleosol, from which phytolith sample one (Phy1) was collected. Laminated carbonaceous shales first occur at 0.75 m in the measured section (Fig. 2), and are interbedded frequently with thin (< 2 cm), very fine sandstone strata, many of which contain asymmetrical ripples. A thick ash occurs from about 2.55 to 3.7 m, and includes trough cross-beds, asymmetrical ripples, and a single horizon of cobbles near the top. Fossil-rich laminated carbonaceous shales comprise the next 8.3 m of deposition, providing the source for all macrofossil horizons reported herein. Irregularly spaced, cm-scale ash beds occur throughout this part of the section, and a thicker (~10 cm) ash is present from 7.55 to 7.65 m. This ash, Level C census stratum, contains leaf compressions, abundant, small, plant fragments, and abundant fish and frog skeletons. Immediately above Level C is a light gray mudstone with abundant and well-preserved fossils of the aquatic fern, *Salvinia* (Fig. 4K). From 12 to 16.7 m, the section is composed of siltstones to fine sandstones, the coarser-grained beds containing burrows or asymmetrical ripples; finer-grained beds often contain plant fossils. The topmost 1.3 m of the section is composed of black, laminated carbonaceous shales.

With the exception of Level C, lithological differences among the macrofossil census horizons are minimal. Viewed with the naked eye, the sedimentary matrix from Level A appears to contain more millimeter-to centimeter-sized fragments of plant material (plant hash) than other stratigraphic levels. In contrast, the matrix from Level F is more uniform, resembling solid, but laminated, chocolate. Levels B through E are intermediate in texture, with no clearly visible trend.

3.2. Macrofossil paleobotany

3.2.1. Floristic composition at Mush

Forty-nine leaf morphotypes are recognized at Mush; ten are represented by a single specimen, and an additional three occur at only one stratigraphic level. Legumes, which are recognized here primarily by the presence of a pulvinus, dominate the Mush flora, making up 16.3% of morphotypes and 76.1% of all leaves (Table 1; Figs. 5 and 6). Between 55.3% (Level A) and 87.4% (Level F) of leaves at individual stratigraphic levels are legumes. Morphotype "Legume 1" is the most abundant leaf taxon by far; it comprises 31% of the flora at Level A, but at least 50% and as much as 66% (Level F) elsewhere (Table 1). Two other legume morphotypes, "Short drip tip" and "Interrupt," are also important in all floras, comprising between 5% and 11% of leaves within a stratigraphic level (Figs. 5 and 6; Table S3).

To examine tropical forest taxonomic turnover through time as might have been caused by environmental perturbations, we analyzed compositional similarities between stratigraphic levels using both presence/absence (Jaccard coefficients) and abundance (NMDS) data. Overall, there is little turnover among stratigraphic levels in the species present or their abundance distribution, with Levels C and A being the most distinct based on abundance distributions (Table 2; Figs. 6 and 7). The average Jaccard coefficient for Level C versus other stratigraphic levels is 0.387, compared with averages of 0.538–0.571 for the other levels (Table 2). Level C also plots farthest from the other sites on the NMDS ordination (Fig. 7), most likely due to the high abundances of a Malvales morphotype (Fig. 8A–D) and *Tacca umerii* (Fig. 4E–G). While the species present at Level A are consistent with all other levels, as indicated by the high average Jaccard coefficient (based upon presence-absence data), the relative abundances of these species differ from those

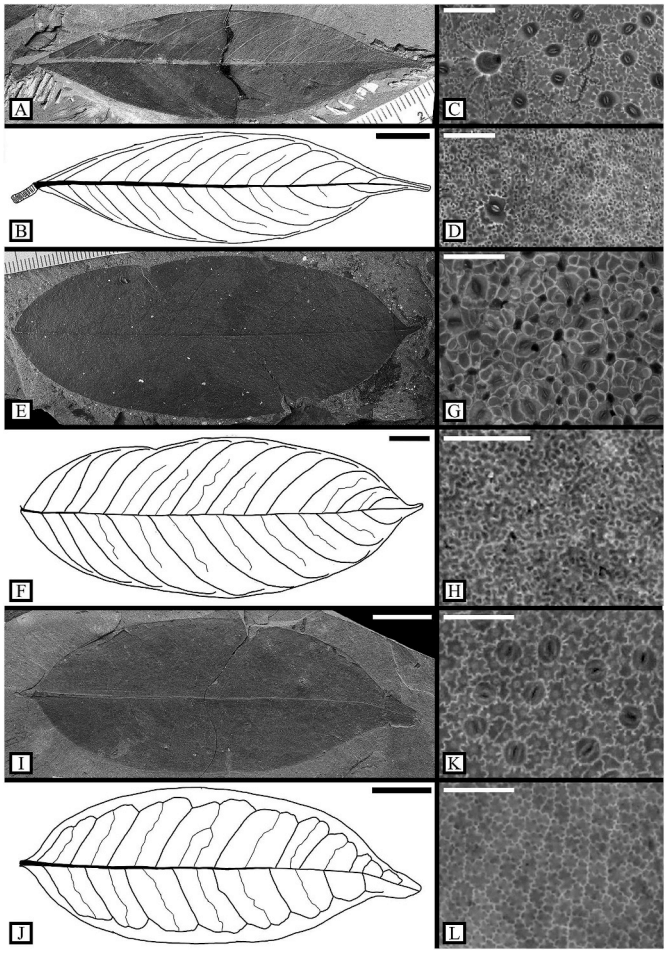

Fig. 5. The three most abundant leaf types at Mush, all of which are legumes. Legume 1 specimen MU29-40B #1 (A) and accompanying line drawing (B). Abaxial (C; MU13-2) and adaxial (D; MU23-37 #1) Legume 1 cuticle. "Short Drip Tip" specimen MU41-54 (E) and accompanying line drawing (F). Abaxial (G; MU23-34) and adaxial (H; MU17-13) "Short Drip Tip" cuticle. "Interrupt" specimen MU27-5 (I) and accompanying line drawing (J). Abaxial (K; MU23-26 #3) and adaxial (L; MU18-4B #2) "Interrupt" cuticle. Line drawings show primary, secondary, and intersecondary veins and demonstrate venation differences among morphotypes. Scale bars in C, D, G, H, K, and L are 50 μm, and scale bars in B, F, I, and J are 1 cm. Tick marks on the rulers in A and E are millimeters.

Table 2
Heterogeneity among stratigraphic levels at Mush, according to the Jaccard similarity coefficient.

	Level A	Level B	Level C	Level D	Level E	Level F	Avg Jaccard
Level A	–						0.57
Level B	0.57	–					0.55
Level C	0.48	0.39	–				0.39
Level D	0.58	0.61	0.34	–			0.54
Level E	0.58	0.62	0.32	0.62	–		0.56
Level F	0.65	0.58	0.39	0.55	0.65	–	0.56

at other levels (Fig. 6). Level A has the lowest abundance of Legume 1, and relatively high abundances of dicot morphotypes "Long&Loopy" (Fig. 8E–G), "Trinverved pulvinate" (Fig. 8H–K), and "Yellow leaf" (Fig. 4A–D) and monocot *Tacca umerii* (Fig. 4E–G). Levels B, D, E, and F have high similarity in both species composition and abundance distributions, with Levels B, E, and F so similar that they overlap one other on the NMDS plot (Fig. 7).

The results from analyses of taxonomic composition and abundances at the individual quarry scale (as an indication of lateral heterogeneity) complement those for combined stratum (Level) results; quarries from Levels B, E, and F have overlapping distributions on the NMDS plot, those from Level D are immediately adjacent to the B, E, F cloud, and quarries from Level A and Level C plot in isolated areas of the NMDS space, but close to one another (Fig. 7). Pairwise distances between all quarries were computed using both Bray-Curtis (abundance data) and Jaccard (based on shared species) indices. Dissimilarity measures between quarries from different stratigraphic levels are significantly higher than dissimilarity measures between quarries from the same stratigraphic level whether using Bray-Curtis or Jaccard indices (Welch Two Sample *t*-test, $p < 0.001$ for Bray-Curtis and $p = 0.001$ for Jaccard).

3.2.2. *Diversity and evenness at Mush*

Floral diversity and evenness vary among stratigraphic levels. Species richness standardized to a count of 300 leaves per level ranges from 20.4 ± 1.7 to 30.9 ± 2.0 (Table 1). Beginning with the lowest sample in the section, Level A has moderate richness, at 25 ± 0.9 taxa. Richness increases for Level B, and reaches a maximum among all levels at 30.9 ± 2.0 for Level D. Richness decreases to a minimum of 20.4 ± 1.7 for Level F (Table 1). Sample size is too small at Level C to get meaningful richness values either for the quarries or the stratum. A similar pattern exists when comparing richness at individual quarries; average richness at 100 leaves is highest at Level D (18.9) and lowest at Level F (12.6), with similar values among A, B, and E. Evenness

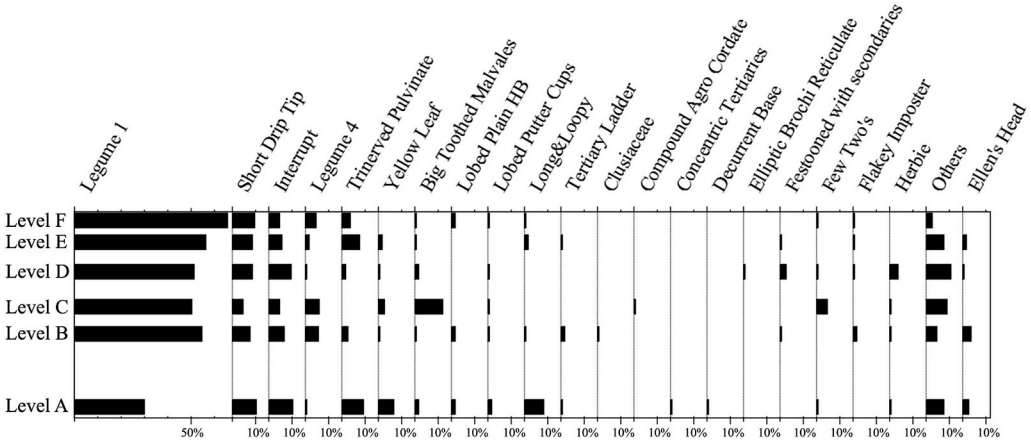

Fig. 6. Relative taxon abundance distributions per stratigraphic level. Morphotypes comprising at least 3% of a stratigraphic level are named individually; the relative abundances of all other morphotypes are summed and shown under "Others." Legume 1, "Short Drip Tip," "Interrupt," and Legume 4 are all legumes; all others are dicots with the exception of "Ellen's Head," which is a monocot. Counts of each leaf morphotype at each stratigraphic level are available in Table S3, and key features of each morphotype are available in Table S6.

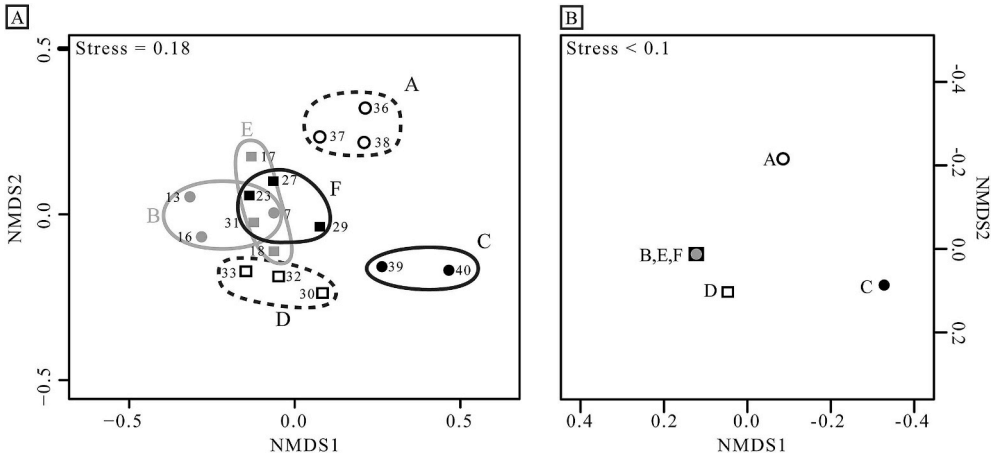

Fig. 7. Nonmetric multidimensional scaling ordination of Mush quarries (A) and stratigraphic levels (B). Axes are reversed in panel B to emphasize the similarity between the grouping of quarries in panel A with that of stratigraphic levels in panel B. Numbers denote sublocalities and letters stratigraphic levels, as illustrated in Fig. 3. Symbols are as follows: Level A data are white circles, Level B gray circles, Level C black circles, Level D white squares, Level E gray squares, Level F black squares. In panel B, Levels B, E, and F plot on top of each other.

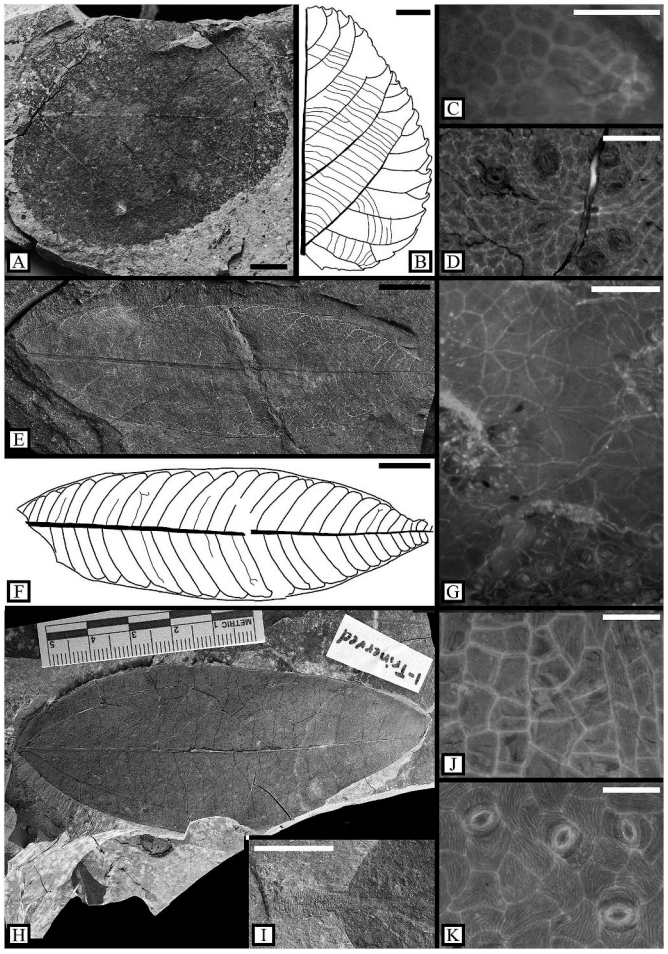

Fig. 8. Morphotypes that occur at relatively high abundance in Level A. Big Toothed Malvales morphotype, specimen MU39-9 (A) with line drawing of secondary and tertiary venation and teeth (B), adaxial cuticle with stellate trichome (C; MU7-43), and abaxial cuticle with stomata and trichome base (D; MU32-28 #1). "Long&Loopy" dicot morphotype, specimen MU37-22 #9 (E) and accompanying line drawing (F). Adaxial cuticle, consisting of elongate cells arranged radially around a trichome base, is shown in the upper two thirds of the panel G, and abaxial cuticle, with closely spaced stomata, is shown in the lower third of panel G (MU29-1 #2). "Trinerved pulvinate" dicot morphotype, specimen MU44-66 (H), pulvinate petiole (or petiolule; I; MU17-29), and adaxial (J; MU29-15) and abaxial cuticle (K; MU29-15). Scale bars are 1 cm in A, B, E, and F, 0.5 cm in I, and 50 μm in C, D, G, J, and K. The ruler in H is in centimeters.

(Pielou's J) is low at all stratigraphic levels and correlates to the proportion of Legume 1 leaves at the stratigraphic level ($R^2 = 0.80$, $p = 0.02$). Levels A and C have the highest evenness. Level B, D, and E are similarly even, and Level F is slightly less even (Table 1). Evenness measures for Level C should be considered with caution due to the relatively low sample size.

Average species richness within a quarry (α_q) at Mush is 20.6 species, which is 42% of the total number of species in the flora. When partitioned additively, average among-quarry richness within a stratigraphic level (β_w^+) is 9.2 species (18.7%), and among stratigraphic level diversity (β_b^+) is 19.2 species (39.3%). Partitioning species richness multiplicatively demonstrates that there are 1.55 distinct communities per stratigraphic level and 1.78 distinct communities among stratigraphic levels. In contrast, when diversity is partitioned using the numbers equivalent of Simpson's index (^2D), a single quarry captures about 92% of the effective number of common species at Mush. Average $\beta_w^\times$ is 1.02 and $\beta_b^\times$ is 1.09, indicating that there is essentially one distinct community of dominant species on the landscape.

3.3. Phytoliths

Out of the 23 samples processed, six yielded bio-silica remains (Table 3). Lacustrine bio-silica remains, consisting mainly of sponges but occasionally also diatoms (sample Phy3, Phy4), occur in five of the samples in percentages ranging from 79% to 96% relative to the total phytolith count (Fig. 2). The exception is sample Phy1, which comes from a paleosol 12 m below the measured section, predating lake formation, and yielding only phytoliths.

Forest indicator (FI) morphotypes, mainly represented by spherical rugose/granulate forms (Fig. 9: 1, 2), are the most abundant phytoliths in all six productive assemblages (Fig. 10). Their abundances vary among samples from 47% in sample Phy4 (15.5 m in the section) up to 94% in Phy5 (16.1 m in the section). Hat-shaped morphotypes linked to palms (Fig. 9: 3) occur in low abundances (8–15%) in samples Phy3, Phy4, and Phy6. Herbaceous plant indicators (GSSCP + NDG + Sedge categories) were observed in all assemblages, but their average abundances do not exceed 12% except in Phy3 (28%) and Phy4 (15%). In particular, Phy3 includes a substantially higher amount of GSSCPs (19%) than all other assemblages (< 9%). The D/(D + P) × 100 index shows a median value of 92%; the highest value (100%) is observed for Phy5, and the lowest value (58%) is observed for Phy3 (Fig. 10). This range of values, Phy3 excluded, compares with those obtained for tropical African forests (Fig. 10).

To provide a more robust assessment of the grass community composition present at the Mush Valley locality, a minimum of 100 GSSCP was counted for the three samples with the highest GSSCP abundances, namely, Phy3 (19% GSSCP of the total phytolith assemblage), Phy4 (7% GSSCP), and Phy6 (8% GSSCP). Because of these

Table 3
Productive phytolith samples.

Sample ID	Field sample number	Meter level in measured section (Fig. 2)	Lithology	Bio-silica remains
Phy6	DDMU-1	17.7	Carbonaceous shale	Sponge, Phytolith
Phy5	DDMU-2	16.1	Carbonaceous shale	Sponge, Phytolith
Phy4	MV10-24	15.5	Laminated black carbonaceous shale	Sponge, Diatom, Phytolith
Phy3	MV10-22	14.9	Laminated black carbonaceous shale	Sponge, Diatom, Phytolith
Phy2	MU-11	1.7	Organic-rich mudstone	Sponge, Phytolith
Phy1	MV10-02	12 m below base of figured section	Paleosol	Phytolith

augmented counts, a total of 26 GSSCP morphotypes were distinguished and described. Three are similar to morphotypes that today are produced by Bambusoideae grasses (Piperno and Pearsall, 1998). These morphotypes consist of spiked top rondels (Fig. 9: 13–15), 4-lobed crosses decorated by bumps on the top surface edges (Fig. 9: 23), and collapsed saddles of two variants (Fig. 9: 11–12). Moreover, the presence of Pharoideae grasses is supported by the combined occurrence of two morphotypes, a trapeziform (Fig. 9: 8–9) and a bilobate (Fig. 9: 10), which both match the features observed for the phytoliths produced by the extant South American genus *Pharus* (Piperno and Pearsall, 1998;

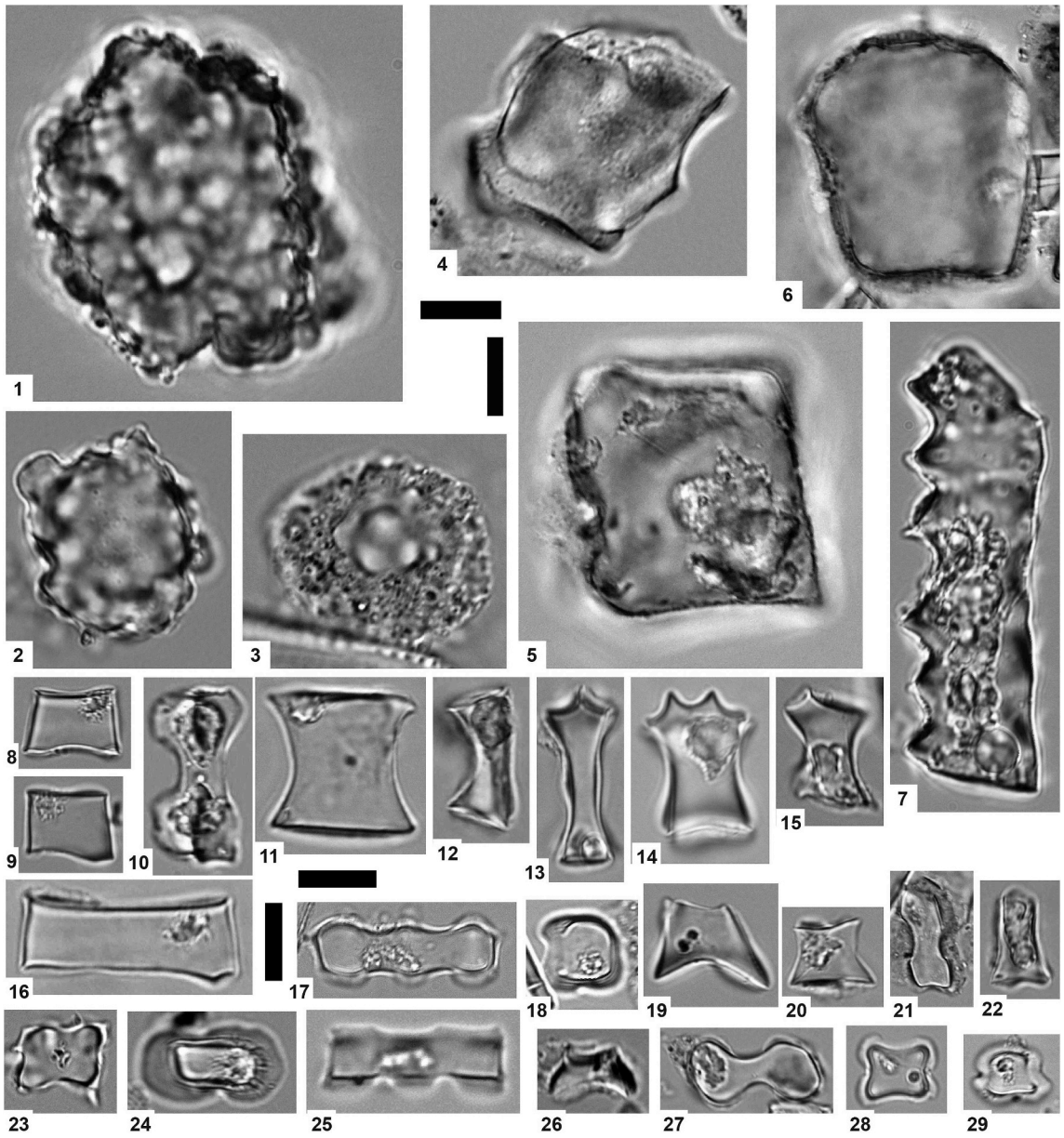

Fig. 9. Photographs of the most abundant and taxonomically significant phytolith morphotypes observed in the Mush Valley samples. Phytolith morphotypes were classified into five categories for paleoenvironmental reconstruction: Grass Silica Short Cell Phytoliths (GSSCPs; panels 8–28), forest indicators (panels 1,2,4), palms (panel 3), non-diagnostic grasses (panels 6, 7), and non-diagnostic other (panel 5). All phytoliths were photographed at the same magnification; scale bars are 10 μm. Additional description and diagnosis of phytolith morphotypes is included in Table S2.

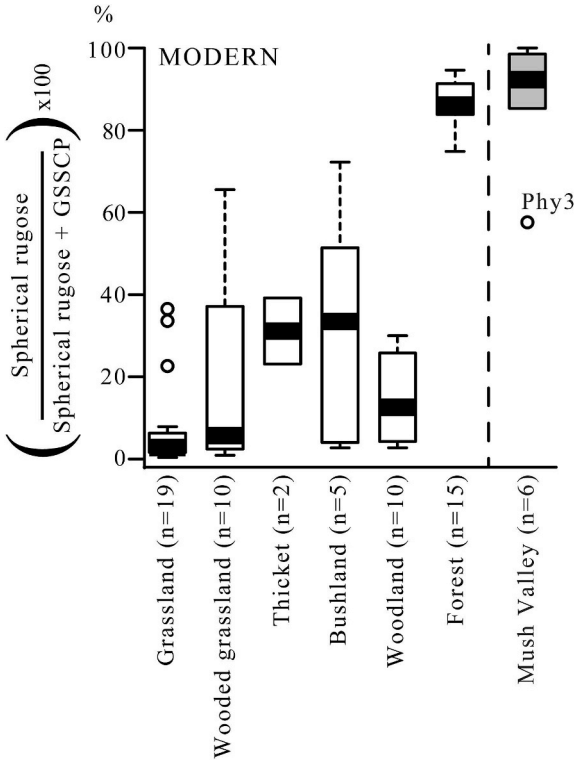

Fig. 10. Ratio between spherical rugose phytoliths and Grass Silica Short Cell Phytoliths (GSSCPs) as an estimation of the vegetation type/physiognomy (modified after the D/P index defined by Bremond et al., 2008) in 66 modern soil phytolith assemblages (Barboni et al., 2007; Novello et al., 2017) compared to the six productive Mush Valley fossil assemblages. The Phy3 assemblage occurs at 14.9 m in the section (Fig. 2). Modern sites were classified into six different vegetation types according to White (1983) classification.

Strömberg, 2003), and, more importantly, the extant African genus *Leptaspis*. Finally, the rare occurrence of polylobates displaying a slightly trapeziform cross section, and true "*Stipa*-type" bilobates (Fig. 9: 24), which were originally described from North American pooids (Fredlund and Tieszen, 1994; Strömberg, 2003) may indicate that the Pooideae subfamily was also represented at this locality. Still, because trapeziform bilobates have also been observed in leaf tissue of other modern African grass subfamilies within the PACMAD clade (Novello et al., 2012), this assignment remains tentative. Similarly, the occurrence of plateaued saddle-like morphotypes (Fig. 9: 18, 26), which are today produced in abundance in the genus *Phragmites* (Piperno and Pearsall, 1998), may point to the presence of C_3 PACMADs in the Arundinoideae. However, it cannot be ruled out that they instead derive from Chloridoideae as plateaued saddle-like GSSCP have been reported from a few species within this subfamily (Neumann et al., 2017; Novello et al., 2012). Moreover, the occurrences of various bilobate and cross types typical of various PACMAD grasses (Fig. 9: 21, 27, 28, 29) likely indicate the presence of the Panicoideae subfamily at Mush. Finally, a number of morphotypes (e.g., Fig. 9: 19, 20, 22) could not be placed taxonomically, mostly because they are known to express high redundancy in modern African grasses.

3.4. Geochemistry

The apolar lipids in Mush sediments contain a suite of well-preserved leaf-wax *n*-alkanes along with pentacyclic, tetracyclic, and occasional tricyclic terpenoids (Fig. S1; Table S5). Preservation of primary leaf wax *n*-alkane distributions is excellent in these sediments as indicated by the ACL and CPI values (Supplemental Information). ACL values range from 29.3 to 31.1 and CPI values from 3.7 to 5.3 (Fig. S2), both of which are consistent with observations from living plants (Bush and McInerney, 2013). No significant differences in ACL or CPI are observed throughout the section (Table S5). The pentacyclic triterpenoids are primarily bacterial hopanes that range in size from C_{27} to C_{33} and include normal and A-ring methyl hopanes. The tetracyclic triterpenoids are primarily des-A-ring degradation products of angiosperm pentacyclic triterpenoids with lupane, and oleanane/ursane structures. A few samples contained tricyclic diterpenoids ($C_{20}H_{36}$) typically ascribed to gymnosperm sources. In addition to the high CPI values, the absence of any sterane or hopane biomarkers indicative of thermal maturation attests to the excellent preservation and thermally immature nature of Mush sediments.

The distribution of *n*-alkane molecules reflects their biological sources and preservation. In general, long chain length *n*-alkane molecules are preferentially sourced from terrestrial plants, and mid-chain length molecules from submerged aquatic plants (Ficken et al., 2000; Liu and Liu, 2016). P_{aq} values measure the relative proportions of longer compared to middle chain lengths and reflect differences in these two sources. The overall contribution of terrestrial plants to the leaf-wax *n*-alkanes is high relative to submerged sources, as indicated by P_{aq} values from 0.04 to 0.20 (Fig. 11), with the proportion of aquatic sources increasing up-section.

Carbon isotope ratios ($\delta^{13}C$) of the terrestrially sourced C_{29} and C_{31}

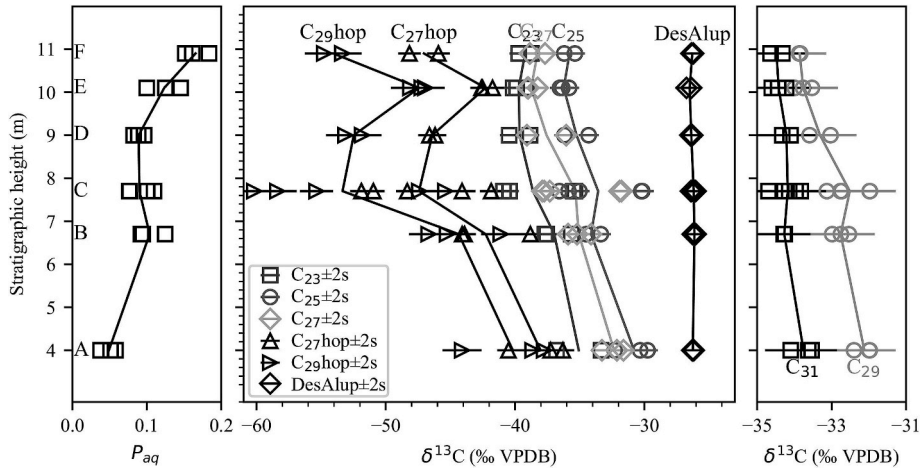

Fig. 11. Stratigraphic evolution of leaf-wax *n*-alkane distributions and leaf-wax, bacterial hopane, and higher plant triterpane carbon isotope values. C_{27}hop is 22,29,30-trisnorhopane, C_{29}hop is 30-norhopane, and DesAlup is Des-A-lupane.

long-chain *n*-alkanes extracted from bulk sediment from plant macrofossil quarries range from −35 to −32‰ and vary by ≤ 2.0‰ throughout the section (Fig. 11; Table S5). These carbon isotope values are similar to the range expected for C_3 angiosperm plants after correction for changes in atmospheric CO_2 (Tipple et al., 2010; Tipple and Pagani, 2010). The $\delta^{13}C$ of des-A-lupane, a degradation product of functionalized angiosperm triterpenoids, is also nearly constant at −26.3 ± 0.2‰ (± 1s) suggesting no change in terrestrial vegetation $\delta^{13}C$ values (Fig. S3). In contrast, the mid-chain length (C_{23} and C_{25}) *n*-alkanes sourced from submerged aquatic angiosperms become significantly more negative up-section, decreasing by ~7‰. Hopane molecules that were also measured, and are sourced from bacteria, exhibit the largest range of $\delta^{13}C$ values: −60 to −36‰. Like the mid-chain *n*-alkanes, the hopane $\delta^{13}C$ values become more negative up-section, however the change is much larger in the hopanes, with 30-norhopane (C_{29}) decreasing by 22.4‰ (Fig. 11). Within-level quarry values are more similar to each other than between-level values for $\delta^{13}C$, as well as for chain-length parameters ACL, CPI, and P_{aq} (Fig. S2).

The $\delta^{13}C$ of mid-chain *n*-alkanes and $\delta^{13}C$ of hopanes are correlated with one another (Fig. S4), suggesting they are both influenced by the amount of methane-derived carbon in the lake system. Both also are correlated with P_{aq}, suggesting that the proportion of submerged versus terrestrial vegetation input to the lake sediments is related to the amount of methane produced in the lake. The common driver of methane production and submerged plant inputs could be changing lake levels. In contrast, terrestrial plant *n*-alkanes (C_{29} and C_{31}) show only small variations up-section and with P_{aq} (Figs. S4 and S5), reflecting that the carbon isotope ratios of leaf waxes from terrestrial plants were not impacted by lake level changes.

4. Discussion

4.1. Lacustrine paleoecology

A paleosol at 12 m below the measured section (Fig. 2) provides evidence of subaerial conditions, consistent with phytolith assemblages from this paleosol which are dominated by forest indicators and lack biosilica from aquatic organisms. The occurrence of ignimbrites between this sample and the start of the measured lacustrine section suggests that an explosive volcanic eruption either created a crater lake, or impeded drainage to form a lake.

Evidence of within-lake conditions comes from the organic-rich nature of the sediments themselves, supported by abundant sponge spicules (94.3%) in Phy2. Lagerstätte-quality preservation, including leaf epidermal stellate hairs (Fig. 4F) and organelle-level preservation of frog skin (Colleary et al., 2015), is usually indicative of anoxic conditions, which retards or prevents organic matter decay by aerobic microbes. Extremely fine laminations present in much of the plant fossil producing strata indicate an absence of bioturbation and the exclusion of aerobic benthic biota. The high abundance of des-A ring triterpenoid molecules in all analyzed organic geochemical samples is also indicative of anoxia, as these molecules are diagenetic products formed by microbial degradation of their functionalized precursors under anoxic conditions (van Bree et al., 2016, and references therein). Furthermore, anoxic sediments are indicated by very negative $\delta^{13}C$ values of several hopanoid compounds suggestive of methanotrophy (Fig. 11). Biogenic methane produced by microbes in anaerobic environments typically has $\delta^{13}C$ values below ~-45‰ (Whiticar, 1999). Oxidative consumption of this methane by methanotrophic bacteria imparts a more negative $\delta^{13}C$ signature to bacteria-derived hopane molecules. The strong ^{13}C depletion amongst the C_{30} and smaller hopanes, but not the C_{31} and larger hopanes, is also consistent with methane consumption. In modern peatlands this same $\delta^{13}C$ pattern is observed where it has been ascribed to a more diverse bacterial source including methanotrophs for the smaller hopanes and a more restricted precursor (primarily bacteriohopanetetrol) and bacterial community for the C_{31} and larger hopanes (Inglis et al., 2019). Methane oxidation was also an important contributor to lake water dissolved inorganic carbon, indicated by the more negative $\delta^{13}C$ values among the mid-chain alkanes produced by aquatic macrophytes.

The lacustrine sediments are interrupted by a relatively thick (~18 cm) ash bed at Level C, which contains several frog and fish skeletons. These remains lack skin compressions found elsewhere in the section (e.g., between 8.4 and 8.6 m) and may reflect increased degradation due to relatively higher oxygen levels, and disruption of stratification in the lake. The floating aquatic fern *Salvinia* occurs in the beds immediately above Level C, perhaps in response to deposition of the ash. Floating aquatics are superior competitors for light, but require high dissolved nutrient levels because they do not have roots. We hypothesize that the rapid deposition of Level C ash, which lacks bedding, brought both organic and inorganic nutrients to the water column. The change in water chemistry that occurred during this time would also have impacted amphibians in the lake, potentially causing a massive die-off as evidenced by abundant frog skeletons on the upper surface of Level C.

Evolution of lake conditions up-section is indicated by changing leaf wax *n*-alkane distributions and carbon isotope ratios. The relative contribution of submerged macrophyte leaf-waxes, documented by the P_{aq} parameter, is low at the base of the lacustrine section (Level A) and increases up-section (Fig. 11). This may indicate shallowing of the lake and increasing proximity to littoral vegetation at the sampling locations. Such decreases in lake depth could result from sedimentary infilling and/or incision of the lake outlet over time. Lake-depth variations due to hydrologic change appear unlikely as reconstructed rainfall amounts do not significantly change up-section (Bush et al., 2017). Methane oxidation also increases up-section as documented in the progressively more negative $\delta^{13}C$ values of bacterial hopanes and aquatic macrophyte leaf-waxes (Fig. 11). It is not certain whether this is a response to shallowing conditions, increasing thickness of organic rich sediments, or other processes.

The sediments above the macrofossil census levels, particularly between 13 and 16.5 m, contain coarser-grained deposits including sandstones with fining upward sequences, burrows, and asymmetrical ripples. These deposits suggest lower lake levels and perhaps stream flow into the lake, in addition to an oxygenated mud-water interface, and may reflect the culmination of the shallowing trend identified in the lacustrine shales. The biosilica assemblages document diatoms at 14.9 m and 15.5 m, suggesting a change in hydrology. Moreover, these assemblages are more heterogeneous, containing a significant proportion of palm phytoliths and grass phytoliths that strongly resemble those produced by Arundinoideae and mesophytic (likely C_3) Panicoideae species, perhaps growing along the lake margin. Although no palm macrofossils were identified in the census collections, *Sclerosperma* pollen (Fig. 4I–K), which is morphologically distinct from other palm genera (Grímsson et al., 2019), was recovered from four stratigraphic levels. Today, *Sclerosperma* most commonly occurs in swampy areas of West Africa (Van Valkenburg et al., 2008).

4.2. Terrestrial paleoecology

To understand how much time could be represented by the 7 m of sedimentary strata from which the plant localities at Levels A - F were collected, we can look to Pleistocene lacustrine core sediments that have good time control through the column. Sedimentation rates in tropical African lakes and swamps vary with depth for a variety of reasons that may include climate change, surrounding vegetation type, and compaction, but overall the rates range from about 20 to 50 yrs/cm (e.g., Marchant et al., 1997; Rucina et al., 2009). Barombi Mbo, Cameroon, a volcanic maar lake surrounded today by lowland tropical forest, has been studied extensively; it exhibits little interruption in sedimentation and has a remarkably consistent rate of deposition for its depth (Giresse et al., 1991; Lebamba et al., 2012; e.g., Maley et al.,

1990). There, 21 m of organic matter has been radiocarbon-dated to 28,000 B.P., producing an overall chronology of about 13 yrs/cm. The deepest dated segment where compression should be the most significant has a chronology of about 10 yrs/cm (Lebamba et al., 2012). Mush Valley sediments are lithified, and therefore compaction and dewatering likely played a large role in the time represented. Deep terrestrial cores from Europe are among the longest known, but even there at depths of 18–20 m, age – depth relationships indicate accumulation times of between 23 and 67 yrs/cm (Lake Yamozero, Russia; Helmens, 2014; La Grande Pile, France; Rousseau et al., 2006). The lacustrine shales at Mush show no signs of hiatuses aside from the short-lived ash deposits. Thus, by analogy with the well-dated lacustrine cores, the 7 m of carbonaceous shale at Mush would have accumulated over the course of millennia, very likely amounting to no longer than 50,000–60,000 years.

Each macrofossil census level is approximately 5 cm thick, which, if the above estimates of accumulation rates are appropriate, would represent as much as one to three centuries. The finely laminated shales and organic preservation indicate very little if any mixing took place once leaves settled to the bottom of the lake. At this scale of time averaging, a single level could sample a community that has been stable and is a mature forest, or a community at some stage of recovery from an intermediate level of disturbance (e.g., from an extreme weather event, tree falls, or eruption and deposition of volcanic ash). An abundance of forest-indicator phytoliths in Phy2 documents that closed forest conditions surrounded the lake before the start of our macrofossil record, and supports the interpretation of Bush et al. (2017) that Mush was a closed-canopy, mixed-moist semi-evergreen forest, based on isotopic, taxonomic, plant morphological, and paleoclimatic data. In addition, phytolith evidence for closed-habitat grass subfamilies such as Pharoideae and Bambusoideae occurring throughout the Mush sequence lends further credence to this reconstruction.

Fine-scale sampling of closely-spaced contemporaneous quarries reflects heterogeneity of the surrounding source vegetation as represented by leaves falling or washing into the lake. The percent of species shared between two quarries from the same stratigraphic level ranges from 38% to 64%, which is only slightly higher than the range of 30%–55% observed between two litter samples from the same hectare of a modern, heterogeneous Peruvian forest (Burnham, 1994). Each fossil assemblage likely represents 100–300 years, and so it is unsurprising that fossil assemblages would be more similar than litter samples collected in the same year. Analyses of between-quarry and between-level similarity indicate that species abundance patterns vary more between levels than between quarries. That is, temporal variation was greater than spatial variation. Additive diversity partitioning analyses support this result: between-level richness (β_b^+) is more than twice as high as between-quarry (within-level, β_w^+) richness. Differences among stratigraphic levels are statistically significant, as indicated by Welch Two Sample *t*-tests using both Bray-Curtis and Jaccard differences. However, comparing richness and the numbers equivalent of Simpson's index demonstrates that there is little change in the dominant species either within or between levels; it is the rarer species that are driving the differences. This is further demonstrated by the Jaccard Similarity Coefficients (Table 2); all levels average between 0.55 and 0.57, excluding Level C.

Comparisons of morphotype abundance distributions indicate that Levels A and C are different from each other, and from all other assemblages by level. The uniqueness of Level C may be due to a low sample count (95 leaves), which limits interpretations. This small sample size is due largely to the matrix, which is not a shale, but a blocky, buff-colored mudstone, likely a devitrified ash, with larger, more intact, specimens dispersed among more abundant plant "hash". Compositionally, Level C differs from others by having multiple specimens of *Tacca umerii* and "Big Toothed Malvales." Today, *Tacca* is associated with understorey vegetation in secondary forests, and its presence in Level C could reflect that habitat. Nevertheless, this interpretation remains tentative. Level A differs from other levels by having lower relative abundances of leaves from legume taxa, especially Legume 1 (30.9%), and greater relative abundances of other taxa, particularly *Tacca umerii*, "Long&Loopy," and "Ellen's Head" (Fig. 6). This pattern results in the higher evenness statistic (Pielou's J) for Level A compared with all others and also underlies its greater Simpson's diversity (Table 1; Fig. 7).

Fluctuations in phytolith assemblage composition through the section, specifically in the abundance of forms diagnostic of palms, grasses, and other herbaceous taxa, point to some temporal variation in the structure of vegetation surrounding the lake. However, it is hard to evaluate how these changes in openness relate to the diversity and evenness changes among plant macrofossils, given that the phytolith and macrofossil assemblages are from different horizons.

There is no evidence for major plant species turnover or changes in vegetation structure during the time represented by the sampled horizons, such as would be found, for example, over a comparable time scale spanning the Pleistocene-Holocene transition. The degree of ecological change through time compares favorably to community ecology dynamics and less so to any significant abiotic drivers such as climate change or catastrophic disturbance (in spite of evidence of significant ash falls). For example, slight changes in openness, as indicated by the phytolith record, may relate to tree gap dynamics, development of grassy wetlands along the shore, or similar small-scale processes. Variations in floral diversity and species relative abundance distributions in both time and space may have been driven by minor differences in the abiotic environment or by ecological drift (neutral processes). The Mush Valley record presented here likely illustrates a dynamic stable state in forest vegetation surrounding the lake 21.7 million years ago and provides another example of forest community resilience to volcanism (Lowe et al., 2018, and references therein; García Massini and Jacobs, 2011).

4.3. Early Miocene ecosystems in the African tropical forest biome

The Mush Valley fossil site is unique with regard to its age and geography. No other plant macrofossil assemblages of comparable age have been reported from tropical Africa, although recent revisions to the geochronology of sediments at Rusinga Island, Kenya, estimate the fossiliferous deposits there range in age from 20 to 17 Ma (Peppe et al., 2011). Rusinga plant fossils consist of fruits and seeds with twigs and thorns (Chesters, 1957; Collinson, 1985; Collinson et al., 2009), *in situ* remains of tree stump casts and roots (Michel et al., 2014), and stratigraphically closely associated leaf impressions, all estimated to be approximately 18 Ma (Maxbauer et al., 2013; Michel et al., 2014). Reconstructions based upon these lines of evidence and the sediments themselves are interpreted as representing a variety of habitats, with an important role for deciduous broad-leaved woodland having a continuous canopy (Collinson et al., 2009), forested areas (Maxbauer et al., 2013; Michel et al., 2014), and riparian environments within a climate having pronounced dry seasons (Maxbauer et al., 2013). The fossils and their meaning at Rusinga differ significantly from what we have described for the Mush Valley paleoflora in this paper, but it is important to note that the Mush fossils may be close to three million years older and higher in elevation. Rusinga is nearly 1300 km to the SSW of the Mush Valley, and today is about 1500 m lower in elevation. While Mush may not have been as high as its modern elevation (2700 m above sea level) due to mid-Miocene uplift of the rift shoulders, it sits atop plateau-forming Oligocene flood basalts and therefore is unlikely to have been lower than 1500 m. The time difference makes it impossible to know whether topographic differences or climatic differences account for different environments at Rusinga and Mush.

The late Oligocene Chilga paleobotanical site at Guang River, dated at 27.23 ± 0.3 (Tesfamichael et al., 2017), is only about 400 km to the NNW of the Mush Valley, sits atop plateau basalts, and is 720 m lower

in elevation than Mush as it would have been in the Miocene. The paleoflora was interpreted to represent a lowland or submontane seasonally or periodically inundated riparian forest having botanical affinities with modern floras of Central, West, and East Africa (Pan, 2007, 2010; Pan et al., 2014; Pan et al., 2010). No leaf morphotype occurs at both Chilga and Mush, which is unsurprising given that the roughly seven million years that separate the two sites saw global warming of at least 2 °C (Tesfamichael et al., 2017) and the establishment of a permanent land connection between Africa and Eurasia (Gheerbrant and Rage, 2006). There are, however, similarities at higher taxonomic levels, which will be the subject of future research. Like Mush, legumes dominate the Guang River flora, comprising 47.6% of leaves and 12.5% of leaf morphotypes (Currano et al., 2011). Species within the genus *Tetracera* (Dilleniaceae), the family Dioscoreaceae, and possibly the genus *Strychnos* (Loganiaceae) occur at low abundances at both sites. Although palms are present at both sites, only pollen and phytoliths of the swamp palm, *Sclerosperma*, occur in common, whereas macrofossil remains from Chilga demonstrate palms were diverse and abundant in the late Oligocene, representing three of the five extant subfamilies (Pan et al., 2006). Modern-day tropical Africa is notably depauperate in palms when compared with the Neotropics and Southeast Asia, and our results, in addition to prior documentation of fossil palms, support hypothesized significant declines in diversity at multiple times during the Cenozoic (Morley, 2000; Pan et al., 2006), considerably pre-dating Pleistocene climate changes. Interestingly, there are no known African Neogene fossil assemblages having a diversity of palms.

The Mush data demonstrate that forest vegetation dominated by C_3 taxa persisted in Ethiopia until at least 21 Ma. However, Mush also provides a unique, first glimpse of the Poaceae lineages that inhabited the African continent during the Cenozoic. Its phytolith assemblages suggest a mix of typical forest grasses (Pharoideae, Bambusoideae) and subfamilies known to contain abundant species that today thrive in open habitats (e.g., Panicoideae, Pooideae). These taxonomically, and potentially ecologically diverse communities may foreshadow the onset of forest fragmentation in East Africa later in the Miocene (Uno et al., 2016).

5. Conclusions

The Mush Valley fossil deposits provide a geologically brief view of mid- to upland, closed-canopy forest with affinities to the West, Central, and East African mixed-moist semi-evergreen rainforests that today exhibit several disjunctions (e.g., Faden, 1974). Initial work on the taxonomy of the Mush flora documents taxa not found today in Ethiopia, as was the case with the older Chilga paleoflora (Pan, 2007). Additional work on the living relatives of the Mush flora will reveal perhaps additional but subtle differences between the late Oligocene and early Miocene, and will provide a more nuanced understanding of the biotic changes that took place across the Paleogene-Neogene boundary in the uplands of the Horn of Africa. Furthermore, as is true today, the Mush Valley in the Miocene was likely higher in altitude than western Kenya, where more open conditions have been documented in some areas (Maxbauer et al., 2013). Multiple lines of evidence indicate anoxic bottom waters in the Mush paleo-lake, which permitted exceptional preservation of organic remains and enabled paleoecological analysis of both the vegetation surrounding the lake and the lake itself. To the best of our knowledge, the integration of leaf macrofossils, pollen, phytoliths, compound-specific organic geochemistry, and stratigraphic data in deep time is unique to this study, and demonstrates the potential of proxy inter-comparison for maximally resolved and robust paleoenvironmental reconstruction.

Declaration of competing interest

The authors declare that they have no known competing financial interests or personal relationships that could have appeared to influence the work reported in this paper.

Acknowledgments

We thank the Authority for Research and Conservation of Cultural Heritage for permission to conduct research in the Mush Valley and the director and staff of the National Museum of Ethiopia, particularly T. Getachew and Y. Assefa, for facilitating the paleobotanical research presented here. We are grateful to the people of Upper and Lower Mush for their hospitality, and to M. Clemens, L. Jacobs, J. Noret, and T. Tesfamichael for field assistance and discussion. Three anonymous reviewers provided constructive comments on our manuscript. Our work was funded by U.S. National Science Foundation grants EAR 1053549 (BFJ), EAR 1052478 (EDC), EAR 1053351 (FAM), and EAR 1253713 (CAES), National Geographic Society CRE 8816-10 (EDC), Marie Curie-Sklodowska IOF 659596 “MACEA” (AN), the Austrian Science Fund, FWF, P29501-B25 (FG), and the Australian Research Council FT110100793 (FAM).

Appendix A. Supplementary data

Supplementary data to this article can be found online at https://doi.org/10.1016/j.palaeo.2019.109425.

References

Alexandre, A., Meunier, J.-D., Lézine, A.-M., Vincens, A., Schwartz, D., 1997. Phytoliths: indicators of grassland dynamics during the late Holocene in intertropical Africa. Palaeogeogr. Palaeoclimatol. Palaeoecol. 136, 213–229.
Barboni, D., Bremond, L., Bonnefille, R., 2007. Comparative study of modern phytolith assemblages from inter-tropical Africa. Palaeogeogr. Palaeoclimatol. Palaeoecol. 246, 454–470.
Bremond, L., Alexandre, A., Hély, C., Guiot, J., 2005. A phytolith index as a proxy of tree cover density in tropical areas: calibration with Leaf Area Index along a forest–-savanna transect in southeastern Cameroon. Glob. Planet. Chang. 45, 277–293.
Bremond, L., Alexandre, A., Wooller, M.J., Hély, C., Williamson, D., Schäfer, P.A., Majule, A., Guiot, J., 2008. Phytolith indices as proxies of grass subfamilies on East African tropical mountains. Glob. Planet. Chang. 61, 209–224.
Burnham, R.J., 1994. Patterns in tropical leaf litter and implications for angiosperm paleobotany. Rev. Palaeobot. Palynol. 81, 99–113.
Bush, R.T., McInerney, F.A., 2013. Leaf wax n-alkane distributions in and across modern plants: implications for paleoecology and chemotaxonomy. Geochem. Cosmochim. Acta 117, 161–179.
Bush, R.T., Wallace, J., Currano, E.D., Jacobs, B.F., McInerney, F.A., Dunn, R.E., Tabor, N.J., 2017. Cell anatomy and leaf $\delta^{13}C$ as proxies for shading and canopy structure in a Miocene forest from Ethiopia. Palaeogeogr. Palaeoclimatol. Palaeoecol. 485, 593–604.
Chao, A., Chiu, C.H., Hsieh, T.C., 2012. Proposing a resolution to debates on diversity partitioning. Ecology 93, 2037–2051.
Chao, A., Chiu, C.H., Jost, L., 2014. Unifying species diversity, phylogenetic diversity, functional diversity, and related similarity and differentiation measures through Hill numbers. Annu. Rev. Ecol. Evol. Syst. 45, 297–324.
Chesters, K.I.M., 1957. The Miocene Flora of Rusinga Island, Lake Victoria, Kenya. vol. 101. Palaeontographica Abt. B, pp. 29–71.
Chorowicz, J., 2005. The east African rift system. J. Afr. Earth Sci. 43, 379–410.
Clarke, J., 2003. The occurrence and significance of biogenic opal in the regolith. Earth Sci. Rev. 60, 175–194.
Colleary, C., Dolocan, A., Gardner, J., Singh, S., Wuttke, M., Rabenstein, R., Habersetzer, J., Schaal, S., Feseha, M., Clemens, M., Jacobs, B.F., Currano, E.D., Jacobs, L.L., Sylvestersen, R.L., Gabbott, S.E., Vinther, J., 2015. Chemical, experimental, and morphological evidence for diagenetically altered melanin in exceptionally preserved fossils. Proc. Natl. Acad. Sci. 112, 12592–12597.
Collinson, M.E., 1985. Revision of East african Miocene floras: a preliminary report. Int. Assoc. Angiosperm Paleobotany Newslett. 8, 4–10.
Collinson, M.E., Andrews, P., Bamford, M.K., 2009. Taphonomy of the early Miocene flora, hiwegi formation, Rusinga Island, Kenya. J. Hum. Evol. 57, 149–162.
Couvreur, T.L., Chatrou, L.W., Sosef, M.S., Richardson, J.E., 2008. Molecular phylogenetics reveal multiple tertiary vicariance origins of the African rain forest trees. BMC Biol. 6, 54.
Currano, E.D., Jacobs, B.F., Pan, A.D., Tabor, N.J., 2011. Inferring ecological disturbance in the fossil record: a case study from the late Oligocene of Ethiopia. Palaeogeogr. Palaeoclimatol. Palaeoecol. 309, 242–252.
Diefendorf, A.F., Mueller, K.E., Wing, S.L., Koch, P.L., Freeman, K.H., 2010. Global patterns in leaf C-13 discrimination and implications for studies of past and future climate. P. Natl. Acad. Sci. U.S.A. 107, 5738–5743.
Dilcher, D.L., 1974. Approaches to identification of angiosperm leaf remains. Bot. Rev. 40, 1–157.
Ducrocq, S., Boisserie, J.-R., 2010. Late Oligocene vertebrate localities from northern Kenya (turkana basin). J. Vertebr. Paleontol. 30, 293–299.
Ellis, B., Daly, D.C., Hickey, L.J., Johnson, K.R., Mitchell, J.D., Wilf, P., Wing, S.L., 2009.

Manual of Leaf Architecture. Cornell University Press, Ithaca, NY.
Ellison, A.M., 2010. Partitioning diversity. Ecology 91, 1962–1963.
Faden, R.B., 1974. East African coastal-West African rain forest disjunctions. In: Lind, E.M., Morrison, M.E.S. (Eds.), East African Vegetation. Longman, London, pp. 202–203.
Ficken, K.J., Li, B., Swain, D.L., Eglinton, G., 2000. An n-alkane proxy for the sedimentary input of submerged/floating freshwater aquatic macrophytes. Org. Geochem. 31, 745–749.
Fredlund, G.G., Tieszen, L.T., 1994. Modern phytolith assemblages from the north American great plains. J. Biogeogr. 21, 321–335.
Friis, I., Demissew, S., Van Breugel, P., 2010. Atlas of the Potential Vegetation of Ethiopia. Det Kongelige Danske Videnskabernes Selskab.
García Massini, J.L., Jacobs, B.F., 2011. The effects of volcanism on Oligocene-age plant communities from the Ethiopian Plateau, and implications for vegetational resilience in a heterogeneous landscape. Rev. Palaeobot. Palynol. 164, 211–222.
Gheerbrant, E., Rage, J.C., 2006. Paleobiogeography of Africa: how distinct from gondwana and laurasia? Palaeogeogr. Palaeoclimatol. Palaeoecol. 241, 224–246.
Giresse, P., Maley, J., Kelts, K., 1991. Sedimentation and paleoenvironment in crater lake Barombi Mbo, Cameroon, during the last 25,000 years. Sediment. Geol. 71, 151–175.
Grímsson, F., Denk, T., Zetter, R., 2008. Pollen, fruits, and leaves of *Tetracentron* (Trochodendraceae) from the Cainozoic of Iceland and western North America and their palaeobiogeographic implications. Grana 47, 1–14.
Grímsson, F., van Valkenburg, J.L.C.H., Wieringa, J.J., Xafis, A., Jacobs, B.F., Zetter, R., 2019. Pollen morphology of the African *Sclerosperma* (Arecaceae). Grana 58, 99–113.
Halbritter, H., Ulrich, S., Grímsson, F., Weber, M., Zetter, R., Hesse, M., Buchner, R., Svojtka, M., Frosch-Radivo, A., 2018. Illustrated Pollen Terminology, second ed. Springer International Publishing.
Harris, E.B., Strömberg, C.A.E., Sheldon, N.D., Smith, S.Y., Vilhena, D.A., 2017. Vegetation response during the lead-up to the middle Miocene warmingevent in the northern rocky mountains, USA. Palaeogeogr. Palaeoclimatol. Palaeoecol. 485, 401–415.
Heck, K.L., van Belle, G., Simberloff, D., 1975. Explicit calculation of the rarefaction diversity measurement and the determination of sufficient sample size. Ecology 56, 1459–1461.
Helmens, K.F., 2014. The Last Interglacial Glacial cycle (MIS 5-2) re-examined based on long proxy records from central and northern Europe. Quat. Sci. Rev. 86, 115–143.
Inglis, G.N., Naafs, B.D.A., Zheng, Y., Schellekens, J., Pancost, R.D., 2019. $\delta^{13}C$ values of bacterial hopanoids and leaf waxes as tracers for methanotrophy in peatlands. Geochem. Cosmochim. Acta 260, 244–256.
Jost, L., 2007. Partitioning diversity into independent alpha and beta components. Ecology 88, 2427–2439.
Kieffer, B., Arndt, N., Lapierre, H., Bastien, F., Bosch, D., Pecher, A., Yirgu, G., Ayalew, D., Weis, D., Jerram, D.A., Keller, F., Meugniot, C., 2004. Flood and shield basalts from Ethiopia: magmas from the African superswell. J. Petrol. 45, 793–834.
Koshnaw, R.I., Stockli, D.F., Schlunegger, F., 2018. Timing of the Arabia-Eurasia continental collision—evidence from detrital zircon U-Pb geochronology of the Red Bed Series strata of the northwest Zagros hinterland, Kurdistan region of Iraq. Geology 47, 47–50.
Lande, R., 1996. Statistics and partitioning of species diversity, and similarity among multiple communities. Oikos 76, 5–13.
Lebamba, J., Vincens, A., Maley, J., 2012. Pollen, vegetation change and climate at Lake Barombi Mbo (Cameroon) during the last ca. 33 000 cal yr BP: a numerical approach. Clim. Past 8, 59–78.
Liu, H., Liu, W., 2016. *n*-Alkane distributions and concentrations in algae, submerged plants and terrestrial plants from the Qinghai-Tibetan Plateau. Org. Geochem. 99, 10–22.
Lowe, A.J., Greenwood, D.R., West, C.K., Galloway, J.M., Sudermann, M., Reichgelt, T., 2018. Plant community ecology and climate on an upland volcanic landscape during the early eocene climatic optimum: McAbee fossil beds, British Columbia, Canada. Palaeogeogr. Palaeoclimatol. Palaeoecol. 511, 433–448.
Macgregor, D., 2015. History of the development of the East African Rift System: a series of interpreted maps through time. J. Afr. Earth Sci. 101, 232–252.
Maclatchy, L., 2004. The oldest ape. Evol. Anthropol. Issues News Rev. 13, 90–103.
Madella, M., Jones, M.K., Echlin, P., Powers-Jones, A., Moore, M., 2009. Plant water availability and analytical microscopy of phytoliths: implications for ancient irrigation in arid zones. Quat. Int. 193, 32–40.
Maley, J., Livingstone, D.A., Giresse, P., Thouveny, N., Brenac, P., Kelts, K., Kling, G., Stager, C., Haag, M., Fournier, M., Bandet, Y., Williamson, D., Zogning, A., 1990. Lithostratigraphy, volcanism, paleomagnetism and palynology of Quaternary lacustrine deposits from Barombi Mbo (west Cameroon) - preliminary-results. J. Volcanol. Geotherm. Res. 42, 319–335.
Marchant, R., Taylor, D., Hamilton, A., 1997. Late Pleistocene and holocene history at mubwindi swamp, southwest Uganda. Quat. Res. 47, 316–328.
Maxbauer, D.P., Peppe, D.J., Bamford, M., McNulty, K.P., Harcourt-Smith, W.E.H., Davis, L.E., 2013. A morphotype catalog and paleoenvironmental interpretations of early Miocene fossil leaves from the Hiwegi Formation, Rusinga Island, Lake Victoria, Kenya. Palaeontol. Electron. 16.
McCune, B., Grace, J.B., 2002. Analysis of Ecological Communities. MjM Software Design, Gleneden Beach, Oregon.
Michel, L.A., Peppe, D.J., Lutz, J.A., Driese, S.G., Dunsworth, H.M., Harcourt-Smith, W.E.H., Horner, W.H., Lehmann, T., Nightingale, S., McNulty, K.P., 2014. Remnants of an ancient forest provide ecological context for Early Miocene fossil apes. Nat. Commun. 5, 3236.
Morley, R.J., 2000. Synthesis to origin and evolution of tropical rain forests. In: Morley, R.J. (Ed.), Origin and Evolution of Tropical Rain Forests. John Wiley and Sons, Chichester, pp. 260–280.
Neumann, K., Fahmy, A.G., Müller-Scheeβel, N., Schmidt, M., 2017. Taxonomic, ecological and paleoecological significance of leaf phytoliths in West African grasses. Quat. Int. 434, 15–32.
Novello, A., 2012. Les phytolithes, marqueurs des environnements mio-pliocènes du Tchad. PhD Thesis. Université de Poitiers.
Novello, A., Barboni, D., Berti-Equille, L., Mazur, J.-C., Poilecot, P., Vignaud, P., 2012. Phytolith signal of aquatic plants and soils in Chad, Central Africa. Rev. Palaeobot. Palynol. 178, 43–58.
Novello, A., Barboni, D., Sylvestre, F., Lebatard, A.-E., Paillès, C., Bourlès, D.L., Likius, A., Mackaye, H.T., Vignaud, P., Brunet, M., 2017. Phytoliths indicate significant arboreal cover at *Sahelanthropus* type locality TM266 in northern Chad and a decrease in later sites. J. Hum. Evol. 106, 66–83.
Oksanen, J., Guillaume Blanchet, F., Friendly, M., Kindt, R., Legendre, P., McGlinn, D., Minchin, P.R., O'Hara, R.B., Simpson, G.L., Solymos, P., Stevens, M.H.H., Szoecs, E., Wagner, H., 2016. Vegan: community ecology package. R package version 2.3-4. http://CRAN.R-project.org/package=vegan.
Pan, A.D., 2007. The Late Oligocene (28-27 Myr) Guang River Flora from the Northwestern Plateau of Ethiopia. Huffington Department of Earth Sciences. Southern Methodist University, Dallas, TX.
Pan, A.D., 2010. Rutaceae leaf fossils from the late Oligocene (27.23 Ma) Guang River flora of northwestern Ethiopia. Rev. Palaeobot. Palynol. 159, 188–194.
Pan, A.D., Currano, E.D., Jacobs, B.F., Feseha, M., Tabor, N., Herendeen, P.S., 2012. Fossil *Newtonia* (fabaceae: mimoseae) seeds from the early Miocene (22-21 Ma) Mush Valley in Ethiopia. Int. J. Plant Sci. 173, 290–296.
Pan, A.D., Jacobs, B.F., Currano, E.D., 2014. Dioscoreaceae fossils from the late Oligocene and early Miocene of Ethiopia. Bot. J. Linn. Soc. 175, 17–28.
Pan, A.D., Jacobs, B.F., Dransfield, J., Baker, W.J., 2006. The fossil history of palms (Arecaceae) in Africa and new records from the Late Oligocene (28-27 Mya) of northwestern Ethiopia. Bot. J. Linn. Soc. 151, 69–81.
Pan, A.D., Jacobs, B.F., Herendeen, P.S., 2010. Detarieae *sensu lato* (fabaceae) from the late Oligocene (27.23 Ma) Guang River flora of north-western Ethiopia. Bot. J. Linn. Soc. 163, 44–54.
Peppe, D.J., Deino, A.L., Mcnulty, K.P., Lehmann, T., Harcourt-Smith, W.E., Dunsworth, H.M., Fox, D.L., 2011. New Age Constraints on the Early Miocene Faunas from Rusinga and Mfangano Islands (Lake Victoria, Kenya), American Journal of Physical Anthropology. Wiley-Blackwell 237-237.
Piperno, D.R., Pearsall, D.M., 1998. The silica bodies of tropical American grasses: morphology, taxonomy, and implications for grass systematics and fossil phytolith identification. Smithson. Contrib. Bot. 85, 1–40.
Plana, V., 2004. Mechanisms and tempo of evolution in the African Guineo-Congolian rainforest. Philos. Trans. R. Soc. Lond. Ser. B Biol. Sci. 359, 1585–1594.
Polissar, P.J., D'Andrea, W.J., 2014. Uncertainty in paleohydrologic reconstructions from molecular δD values. Geochimica et Cosmochimica Acta 129, 146–156. https://doi.org/10.1016/j.gca.2013.12.021.
Rasmussen, D.T., Gutierrez, M., 2009. A mammalian fauna from the late Oligocene of northwestern Kenya. Palaeontographica Abteilung a-Palaozoologie-Stratigraphie 288, 1–52.
Rousseau, D.D., Hatte, C., Guiot, J., Duzer, D., Schevin, P., Kukla, G., 2006. Reconstruction of the Grande Pile Eemian using inverse modeling of biomes and delta C-13. Quat. Sci. Rev. 25, 2806–2819.
Rucina, S.M., Muiruri, V.M., Kinyanjui, R.N., McGuiness, K., Marchant, R., 2009. Late Quaternary vegetation and fire dynamics on Mount Kenya. Palaeogeogr. Palaeoclimatol. Palaeoecol. 283, 1–14.
Sangster, A.G., Parry, D.W., 1969. Some factors in relation to bulliform cell silicification in the grass leaf. Ann. Bot. 33, 315–323.
Sosef, M.S., 1996. In: Van Der Maesen, L.J.G., Van Der Burgt, X.M., Van Medenbach De Roy, J.M. (Eds.), Begonias and African Rain Forest Refuges: General Aspects and Recent Progress. Kluwer, Dordrecht, pp. 602–611.
Strömberg, C.A., Dunn, R.E., Madden, R.H., Kohn, M.J., Carlini, A.A., 2013. Decoupling the spread of grasslands from the evolution of grazer-type herbivores in South America. Nat. Commun. 4, 1478.
Strömberg, C.A.E., 2003. The Origin and Spread of Grass-Dominated Ecosystems during the Tertiary of North America and How it Relates to the Evolution of Hypsodonty in Equids, Integrative Biology. University of California, Berkeley.
Strömberg, C.A.E., 2004. Using phytolith assemblages to reconstruct the origin and spread of grass-dominated habitats in the great plains of North America during the late Eocene to early Miocene. Palaeogeogr. Palaeoclimatol. Palaeoecol. 207, 239–275.
Strömberg, C.A.E., 2005. Decoupled taxonomic radiation and ecological expansion of open-habitat grasses in the Cenozoic of North America. Proc. Natl. Acad. Sci. U.S.A. 102, 11980–11984.
Strömberg, C.A.E., Dunn, R.E., Crifò, C., Harris, E.B., 2018. Phytoliths in paleoecology: analytical considerations, current use, and future directions. In: Croft, D.A., Su, F.D., Simpson, S.W. (Eds.), Methods in Paleoecology: Reconstructing Cenozoic Terrestrial Environments and Ecological Communities. Springer International Publishing, pp. 235–287.
Tesfamichael, T., Jacobs, B.F., Tabor, N.J., Michel, L., Currano, E.D., Feseha, M., Barclay, R., Kappelman, J., Schmitz, M., 2017. Settling the issue of "decoupling" between atmospheric carbon dioxide and global temperature: $[CO_2]_{atm}$ reconstructions across the warming Paleogene-Neogene divide. Geology 45, 999–1002.
Tipple, B.J., Meyers, S.R., Pagani, M., 2010. Carbon isotope ratio of Cenozoic CO2: a comparative evaluation of available geochemical proxies. Paleoceanography 25.
Tipple, B.J., Pagani, M., 2010. A 35 Myr North American leaf-wax compound-specific carbon and hydrogen isotope record: implications for C-4 grasslands and hydrologic cycle dynamics. Earth Planet. Sci. Lett. 299, 250–262.
Tolley, K.A., Tilbury, C.R., Measey, G.J., Menegon, M., Branch, W.R., Matthee, C.A., 2011.

Ancient forest fragmentation or recent radiation? Testing refugial speciation models in chameleons within an African biodiversity hotspot. J. Biogeogr. 38, 1748–1760.
Uno, K.T., Polissar, P.J., Jackson, K.E., deMenocal, P.B., 2016. Neogene biomarker record of vegetation change in eastern Africa. Proc. Natl. Acad. Sci. 113, 6355–6363.
van Bree, L.G.J., Rijpstra, W.I.C., Al-Dhabi, N.A., Verschuren, D., Damste, J.S.S., de Leeuw, J.W., 2016. Des-A-lupane in an East African lake sedimentary record as a new proxy for the stable carbon isotopic composition of C-3 plants. Org. Geochem. 101, 132–139.
Van Valkenburg, J., Sunderland, T., Couvreur, T., 2008. A revision of the genus Sclerosperma (Arecaceae). Kew Bull. 63, 75–86.
White, F., 1983. The Vegetation of Africa, a Descriptive Memoir to Accompany the UNESCO/AETFAT/UNSO Vegetation Map of Africa (3 Plates, Northwestern Africa, Northeastern Africa, and Southern Africa, 1: 5,000,000). Unesco, Paris.
Whiticar, M.J., 1999. Carbon and hydrogen isotope systematics of bacterial formation and oxidation of methane. Chem. Geol. 161, 291–314.
Zachos, J.C., Dickens, G.R., Zeebe, R.E., 2008. An early Cenozoic perspective on greenhouse warming and carbon-cycle dynamics. Nature 451, 279–283.
Zetter, R., 1989. Methodik und Bedeutung einer routinemäßig kombinierten lichtmikroskopischen und rasterelektonenmikroskopischen Untersuchung fossiler Mikrofloren. Cour. Forschungsinst. Senckenberg 109, 41–50.